Electronic Supplementary Material (ESI) for Dalton Transactions.

Electrocatalytic reduction of dioxygen by Mn(III) *meso*-Tetra(*N*-methylpyridinium-4-yl) porphyrin in universal buffer

Supporting Information

*Lauren E. Lieske, Shelby L. Hooe, Asa W. Nichols, and Charles W. Machan**

* - machan@virginia.edu; ORCID 0000–0002-5182-1138

Department of Chemistry, University of Virginia, McCormick Road, P.O. Box 400319, Charlottesville, VA, 22904-4319, United States

Table S1. Solutions utilized in this study.

pH Range	Solution
1	1 M HCl and 0.1 M NaCl
2-13	0.04 M Britton-Robinson Buffer[1]
14	1 M KOH and 0.1 M NaCl

Table S2. Electrochemical characterization of the Mn(III)/(II) reduction in a pH 1 solution (1 M HCl /0.1 M NaCl) under Ar saturation conditions as the scan rate is increased.

Scan Rate (V s^{-1})	$E_{1/2}$ vs. NHE (V)	ΔE vs. NHE (mV)	i_{pc}/i_{pa}
0.1	+0.09	299	1.60
0.2	+0.08	326	1.50
0.3	+0.07	342	1.60
0.5	+0.06	371	1.80
1.0	+0.04	453	1.80

Table S3. Electrochemical characterization of the Mn(III)/(II) reduction in pH 3 Britton-Robinson Buffer solution under Ar saturation conditions as the scan rate is increased.

Scan Rate (V s^{-1})	$E_{1/2}$ vs. NHE (V)	ΔE vs. NHE (mV)	i_{pc}/i_{pa}
0.1	0.00	226	1.10
0.2	+0.01	292	1.20
0.3	0.00	318	1.20
0.5	0.00	368	1.20
1.0	0.00	412	1.20

Table S4. Electrochemical characterization of the Mn(III)/(II) reduction in pH 4 Britton-Robinson Buffer solution under Ar saturation conditions as the scan rate is increased.

Scan Rate (V s^{-1})	$E_{1/2}$ vs. NHE (V)	ΔE vs. NHE (mV)	i_{pc}/i_{pa}
0.1	0.00	238	0.99
0.2	0.00	280	1.03
0.3	–0.01	324	1.10
0.5	–0.02	352	1.12
1.0	–0.03	415	1.26

Table S5. Electrochemical characterization of the Mn(III)/(II) reduction in pH 5 Britton-Robinson Buffer solution under Ar saturation conditions as the scan rate is increased.

Scan Rate (V s^{-1})	$E_{1/2}$ vs. NHE (V)	ΔE vs. NHE (mV)	i_{pc}/i_{pa}
0.1	+0.02	167	0.92
0.2	+0.02	193	0.95
0.3	+0.02	215	0.95
0.5	+0.01	246	1.00
1.0	+0.01	290	1.05

Table S6. Electrochemical characterization of the Mn(III)/(II) reduction in pH 6 Britton-Robinson Buffer solution under Ar saturation conditions as the scan rate is increased.

Scan Rate (V s^{-1})	$E_{1/2}$ vs. NHE (V)	ΔE vs. NHE (mV)	i_{pc}/i_{pa}
0.1	+0.02	132	1.10
0.2	+0.02	156	1.05
0.3	+0.02	165	1.05
0.5	+0.02	189	1.05
1.0	+0.01	237	1.05

Table S7. Electrochemical characterization of the Mn(III)/(II) reduction in pH 7 Britton-Robinson Buffer solution under Ar saturation conditions as the scan rate is increased.

Scan Rate (V s^{-1})	$E_{1/2}$ vs. NHE (V)	ΔE vs. NHE (mV)	i_{pc}/i_{pa}
0.1	+0.02	114	0.92
0.2	+0.02	120	0.92
0.3	+0.02	134	0.88
0.5	+0.02	146	0.89
1.0	+0.01	170	0.92

Table S8. Electrochemical characterization of the Mn(III)/(II) reduction in pH 8 Britton-Robinson Buffer solution under Ar saturation conditions as the scan rate is increased.

Scan Rate (V s^{-1})	$E_{1/2}$ vs. NHE (V)	ΔE vs. NHE (mV)	i_{pc}/i_{pa}
0.1	+0.02	86	1.01
0.2	+0.02	94	1.01
0.3	+0.02	95	0.98
0.5	+0.02	103	1.00
1.0	+0.02	119	1.03

Table S9. Electrochemical characterization of the Mn(III)/(II) reduction in pH 9 Britton-Robinson Buffer solution under Ar saturation conditions as the scan rate is increased.

Scan Rate (V s^{-1})	$E_{1/2}$ vs. NHE (V)	ΔE vs. NHE (mV)	i_{pc}/i_{pa}
0.1	+0.02	110	0.99
0.2	+0.02	126	0.98
0.3	+0.02	139	0.99
0.5	+0.02	155	1.00
1.0	+0.01	186	1.03

Table S10. Electrochemical characterization of the Mn(III)/(II) reduction in pH 10 Britton-Robinson Buffer solution under Ar saturation conditions as the scan rate is increased.

Scan Rate (V s^{-1})	$E_{1/2}$ vs. NHE (V)	ΔE vs. NHE (mV)	i_{pc}/i_{pa}
0.1	+0.02	84	0.95
0.2	+0.02	94	0.97
0.3	+0.02	97	0.96
0.5	+0.02	105	0.96
1.0	+0.02	112	0.99

Table S11. Electrochemical characterization of the Mn(III)/(II) reduction in pH 11 Britton-Robinson Buffer solution under Ar saturation conditions as the scan rate is increased.

Scan Rate (V s^{-1})	$E_{1/2}$ vs. NHE (V)	ΔE vs. NHE (mV)	i_{pc}/i_{pa}
0.1	+0.01	75	1.10
0.2	+0.01	82	0.99
0.3	+0.01	88	1.00
0.5	+0.01	97	0.97
1.0	+0.01	107	0.94

Table S12. Electrochemical characterization of the Mn(III)/(II) reduction in pH 12 Britton-Robinson Buffer solution under Ar saturation conditions as the scan rate is increased.

Scan Rate (V s^{-1})	$E_{1/2}$ vs. NHE (V)	ΔE vs. NHE (mV)	i_{pc}/i_{pa}
0.1	–0.02	77	1.30
0.2	–0.03	86	1.31
0.3	–0.03	91	1.22
0.5	–0.03	100	1.17
1.0	–0.02	107	1.09

Table S13 Electrochemical characterization of the Mn(III)/(II) reduction in pH 13 Britton-Robinson Buffer solution under Ar saturation conditions as the scan rate is increased.

Scan Rate (V s^{-1})	$E_{1/2}$ vs. NHE (V)	ΔE vs. NHE (mV)	i_{pc}/i_{pa}
0.1	–0.05	125	1.08
0.2	–0.07	126	1.06
0.3	–0.08	128	1.02
0.5	–0.08	129	1.06
1.0	–0.08	130	1.04

Table S14. Electrochemical characterization of the Mn(III)/(II) reduction in pH 14 Britton-Robinson Buffer solution under Ar saturation conditions as the scan rate is increased.

Scan Rate (V s^{-1})	$E_{1/2}$ vs. NHE (V)	ΔE vs. NHE (mV)	i_{pc}/i_{pa}
0.1	–0.11	223	1.14
0.2	–0.12	235	1.15
0.3	–0.12	244	1.19
0.5	–0.12	254	1.25
1.0	–0.12	249	1.40

Table S15. Electrochemical characterization of Mn(IV)/(III) feature from pH 10-14, CVs taken at a scan rate of 100 mV/s under Ar saturation conditions.

pH	$E_{1/2}$ vs. NHE (V)	ΔE vs. NHE (mV)	i_{pc}/i_{pa}
10	+0.65	250	0.81
11	+0.53	110	1.08
12	+0.39	70	1.05
13	+0.32	70	1.00
14	+0.24	120	1.15

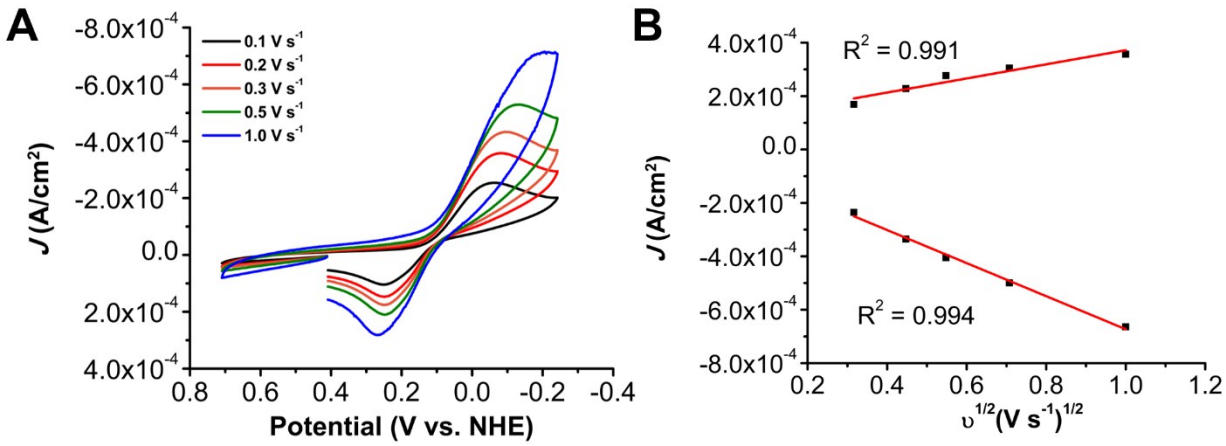

Figure S1. (A) Variable scan rate CVs **(B)** Linear fit demonstrating a homogenous response of $[Mn(TMPyP)Cl]^{4+}$. Conditions: 1 mM $[Mn(TMPyP)Cl]^{4+}$ in a pH 1 (1 M HCl /0.1 M NaCl) solution under Ar saturation conditions, glassy carbon working electrode, glassy carbon counter electrode, 3.0 M NaCl Ag/AgCl reference electrode; varied scan rate.

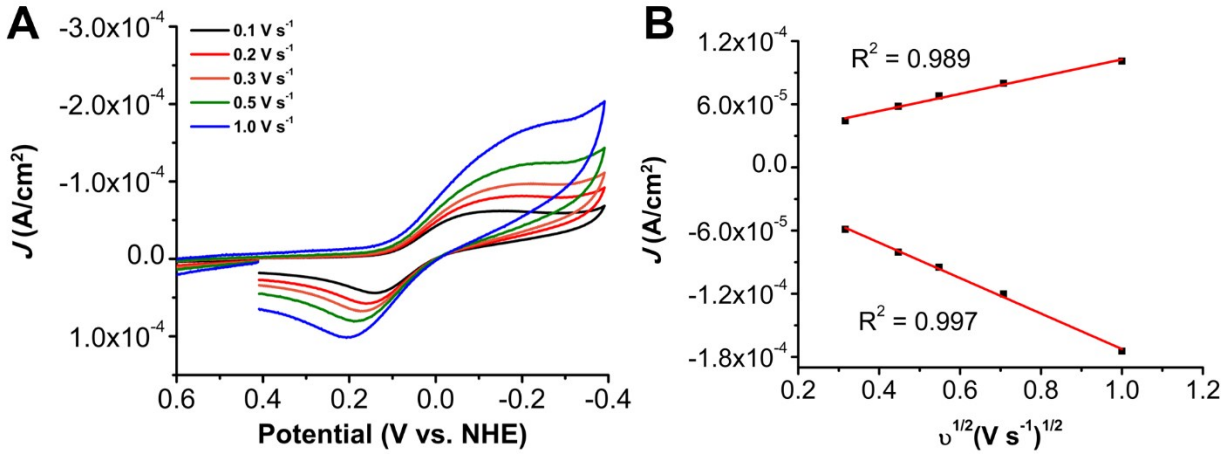

Figure S2. (A) Variable scan rate CVs **(B)** Linear fit demonstrating a homogenous response of $[Mn(TMPyP)Cl]^{4+}$. Conditions: 1 mM $[Mn(TMPyP)Cl]^{4+}$ in a pH 3 Britton-Robinson Buffer solution under Ar saturation conditions, glassy carbon working electrode, glassy carbon counter electrode, 3.0 M NaCl Ag/AgCl reference electrode; varied scan rate.

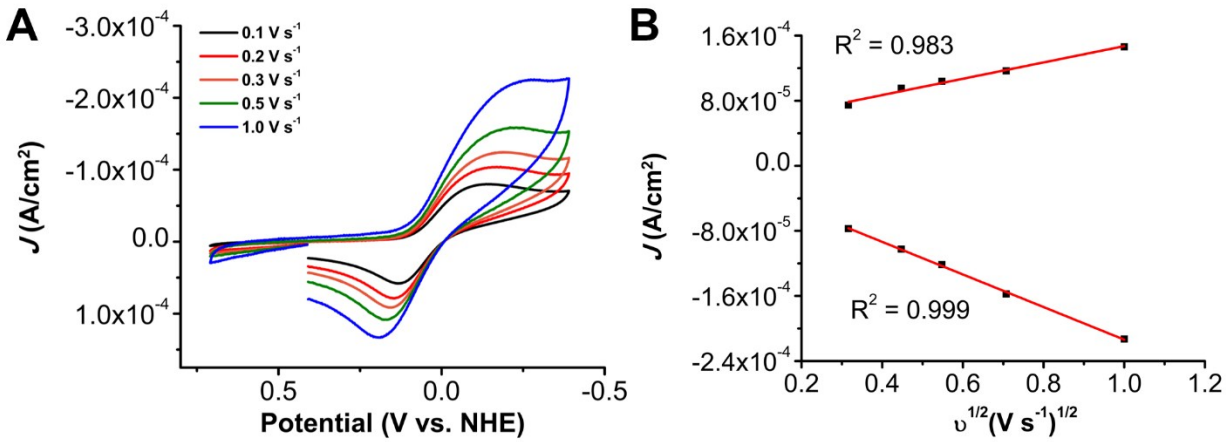

Figure S3. (A) Variable scan rate CVs **(B)** Linear fit demonstrating a homogenous response of $[Mn(TMPyP)Cl]^{4+}$. Conditions: 1 mM $[Mn(TMPyP)Cl]^{4+}$ in a pH 4 Britton-Robinson Buffer solution under Ar saturation conditions, glassy carbon working electrode, glassy carbon counter electrode, 3.0 M NaCl Ag/AgCl; varied scan rate.

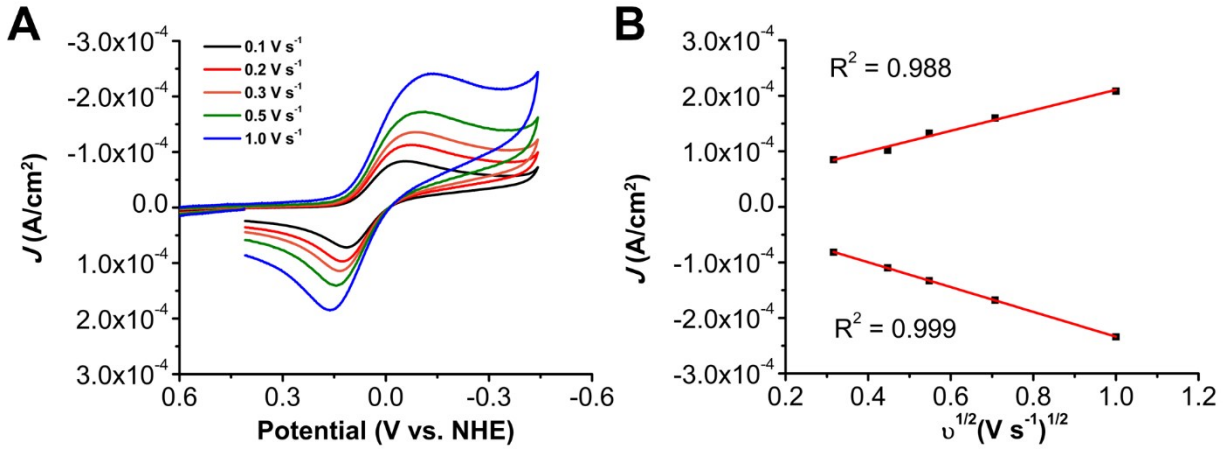

Figure S4. (A) Variable scan rate CVs **(B)** Linear fit demonstrating a homogenous response of $[Mn(TMPyP)Cl]^{4+}$. Conditions: 1 mM $[Mn(TMPyP)Cl]^{4+}$ in a pH 5 Britton-Robinson Buffer solution under Ar saturation conditions, glassy carbon working electrode, glassy carbon counter electrode, 3.0 M NaCl Ag/AgCl reference electrode; varied scan rate.

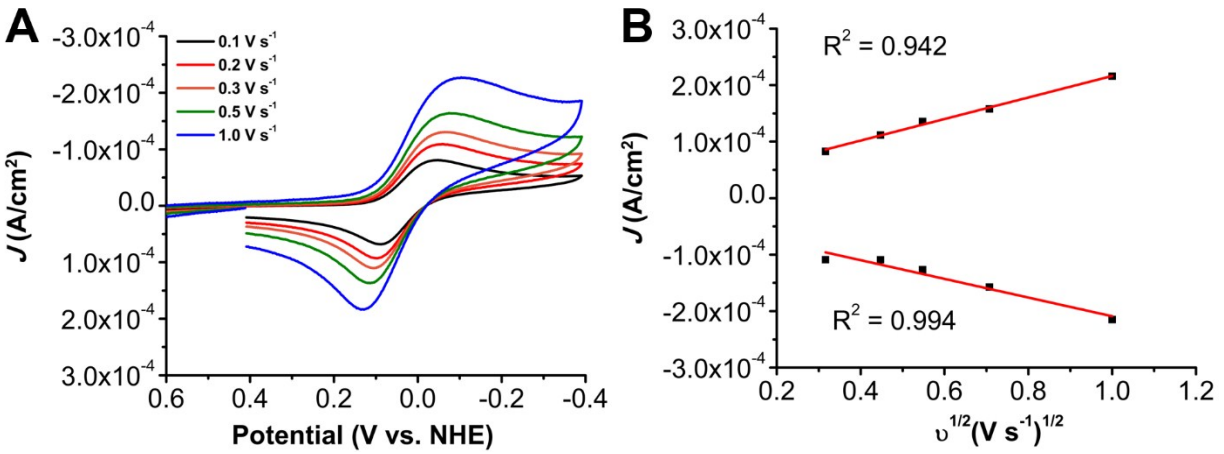

Figure S5. (A) Variable scan rate CVs **(B)** Linear fit demonstrating a homogenous response of $[Mn(TMPyP)Cl]^{4+}$. Conditions: 1 mM $[Mn(TMPyP)Cl]^{4+}$ in a pH 6 Britton-Robinson Buffer solution under Ar saturation conditions, glassy carbon working electrode, glassy carbon counter electrode, 3.0 M NaCl Ag/AgCl reference electrode; varied scan rate.

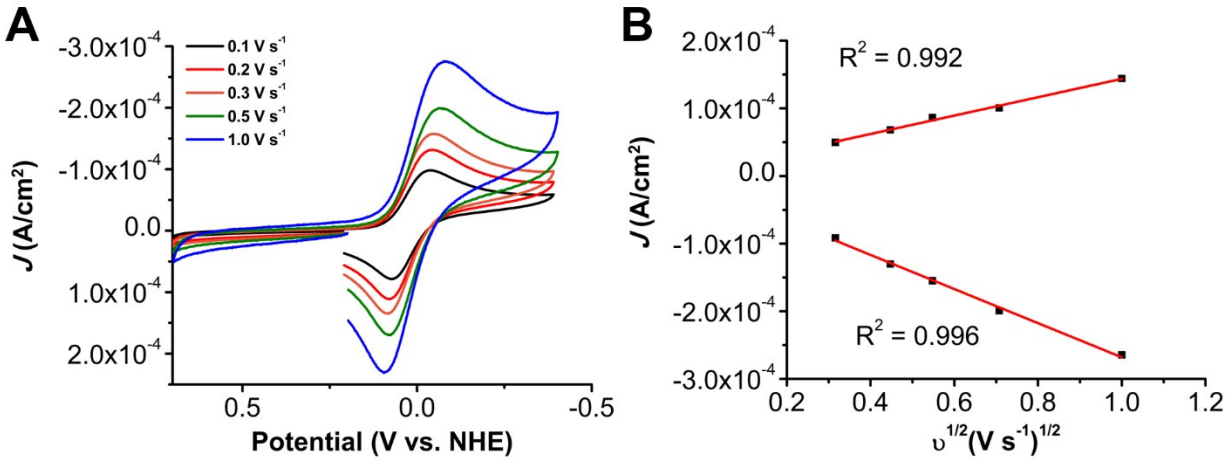

Figure S6. (A) Variable scan rate CVs **(B)** Linear fit demonstrating a homogenous response of $[Mn(TMPyP)Cl]^{+}$. Conditions: 1 mM $[Mn(TMPyP)Cl]^{4+}$ in a pH 7 Britton-Robinson Buffer solution under Ar saturation conditions, glassy carbon working electrode, glassy carbon counter electrode, 3.0 M NaCl Ag/Ag4Cl reference electrode; varied scan rate.

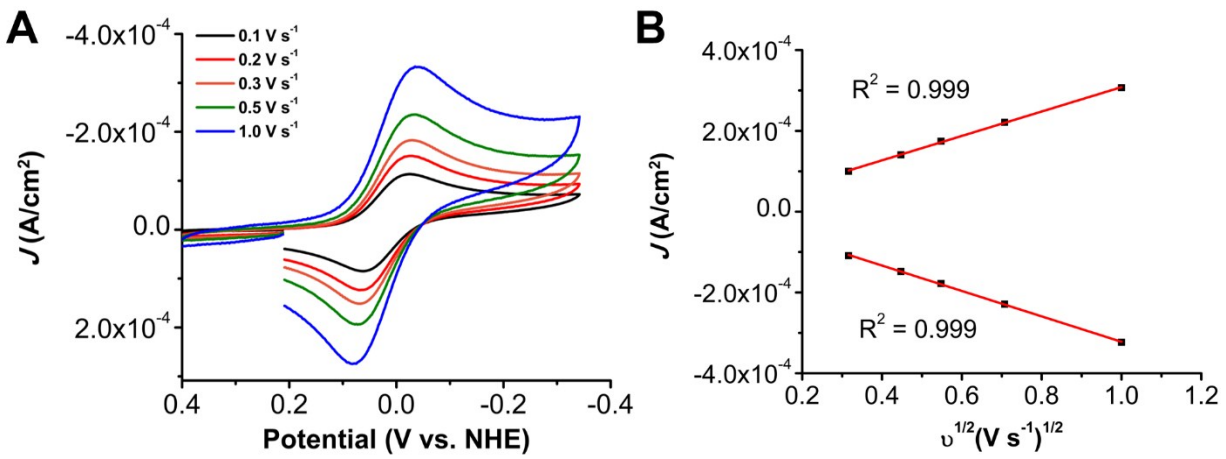

Figure S7. (A) Variable scan rate CVs **(B)** Linear fit demonstrating a homogenous response of $[Mn(TMPyP)Cl]^{4+}$. Conditions: 1 mM $[Mn(TMPyP)Cl]^{4+}$ in a pH 8 Britton-Robinson Buffer solution under Ar saturation conditions, glassy carbon working electrode, glassy carbon counter electrode, 3.0 M NaCl Ag/AgCl reference electrode; varied scan rate.

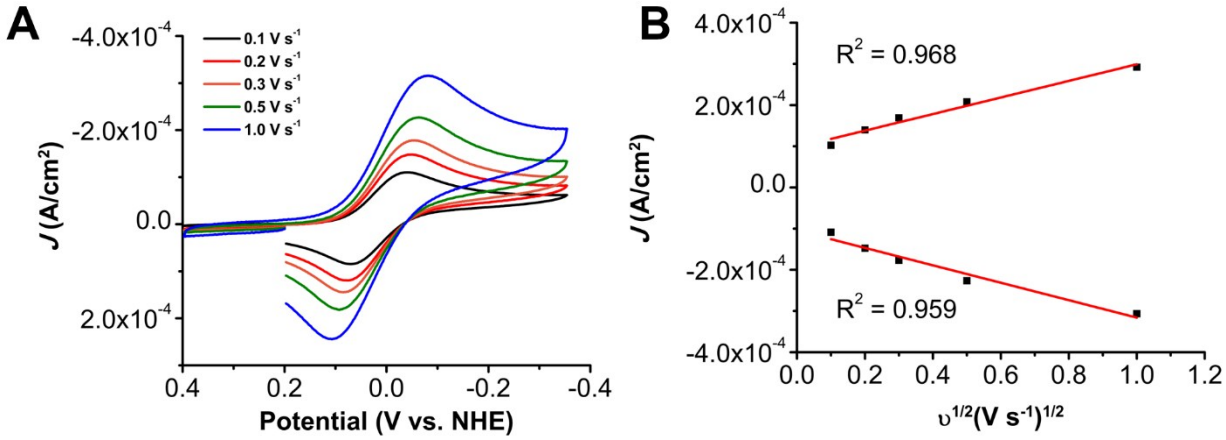

Figure S8. (A) Variable scan rate CVs **(B)** Linear fit demonstrating a homogenous response of $[Mn(TMPyP)Cl]^{4+}$. Conditions: 1 mM $[Mn(TMPyP)Cl]^{4+}$ in a pH 9 Britton-Robinson Buffer solution under Ar saturation conditions, glassy carbon working electrode, glassy carbon counter electrode, 3.0 M NaCl Ag/AgCl reference electrode; varied scan rate.

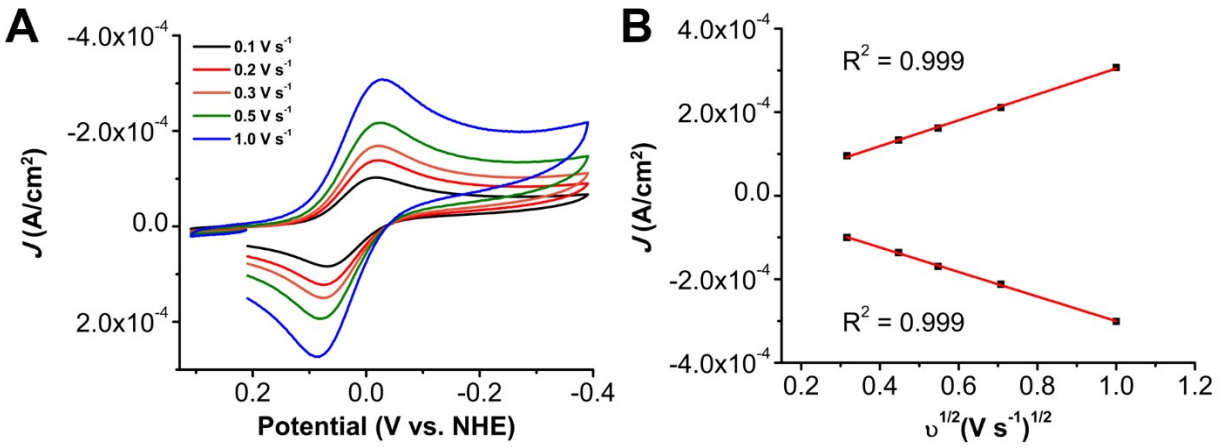

Figure S9. (A) Variable scan rate CVs **(B)** Linear fit demonstrating a homogenous response of $[Mn(TMPyP)Cl]^{4+}$. Conditions: 1 mM $[Mn(TMPyP)Cl]^{4+}$ in a pH 10 Britton-Robinson Buffer solution under Ar saturation conditions, glassy carbon working electrode, glassy carbon counter electrode, 3.0 M NaCl Ag/AgCl reference electrode; varied scan rate.

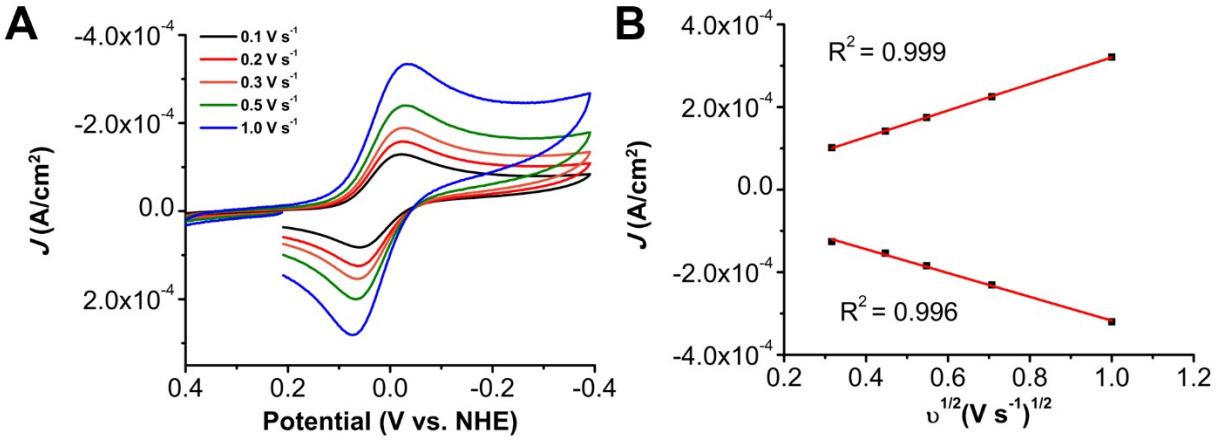

Figure S10. (A) Variable scan rate CVs **(B)** Linear fit demonstrating a homogenous response of $[Mn(TMPyP)Cl]^{4+}$. Conditions: 1 mM $[Mn(TMPyP)Cl]^{4+}$ in a pH 11 Britton-Robinson Buffer solution under Ar saturation conditions, glassy carbon working electrode, glassy carbon counter electrode, 3.0 M NaCl Ag/AgCl reference electrode; varied scan rate.

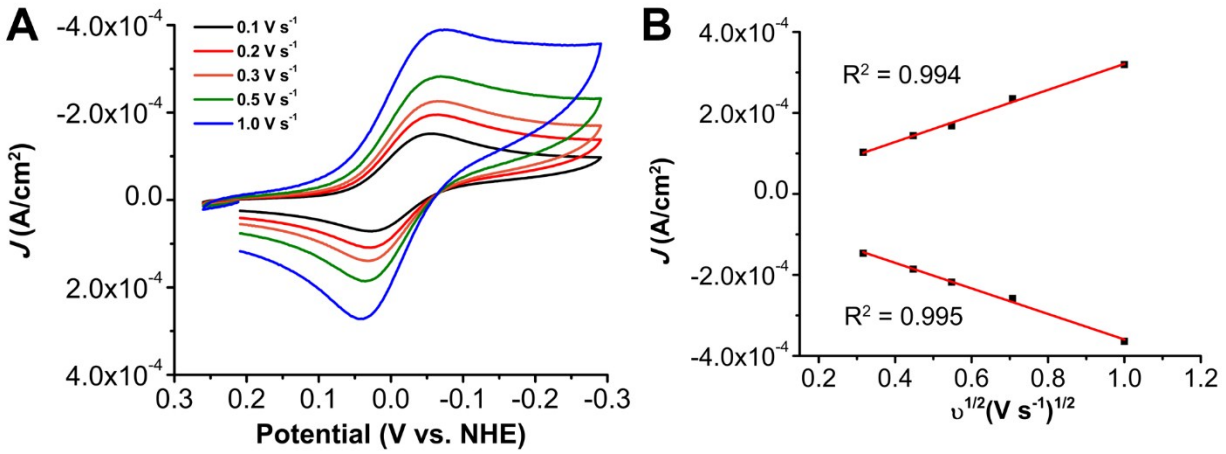

Figure S11. (A) Variable scan rate CVs **(B)** Linear fit demonstrating a homogenous response of $[Mn(TMPyP)Cl]^{4+}$. Conditions: 1 mM $[Mn(TMPyP)Cl]^{4+}$ in a pH 12 Britton-Robinson Buffer solution under Ar saturation conditions, glassy carbon working electrode, glassy carbon counter electrode, 3.0 M NaCl Ag/AgCl reference electrode; varied scan rate.

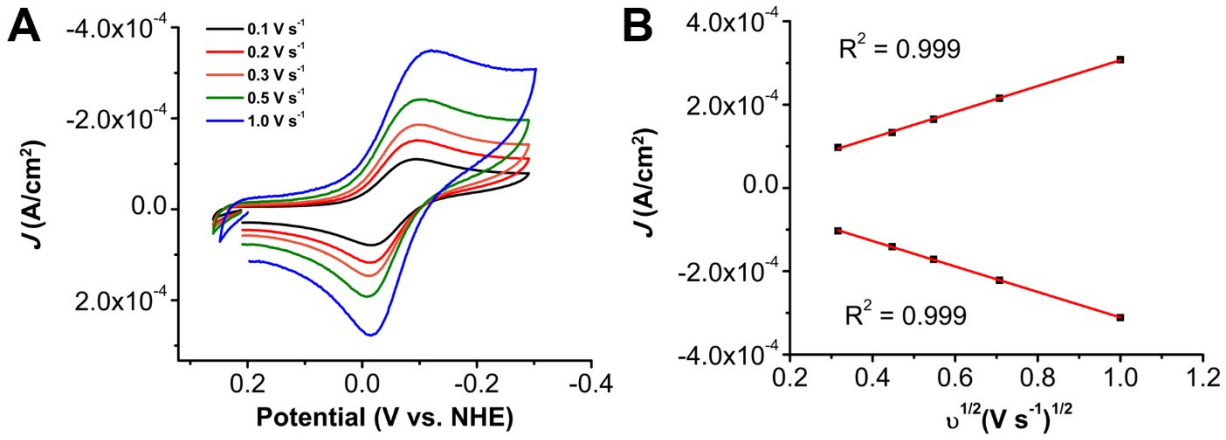

Figure S12. (A) Variable scan rate CVs **(B)** Linear fit demonstrating a homogenous response of $[Mn(TMPyP)Cl]^{4+}$. Conditions: 1 mM $[Mn(TMPyP)Cl]^{4+}$ in a pH 13 Britton-Robinson Buffer solution under Ar saturation conditions, glassy carbon working electrode, glassy carbon counter electrode, 3.0 M NaCl Ag/AgCl reference electrode; varied scan rate.

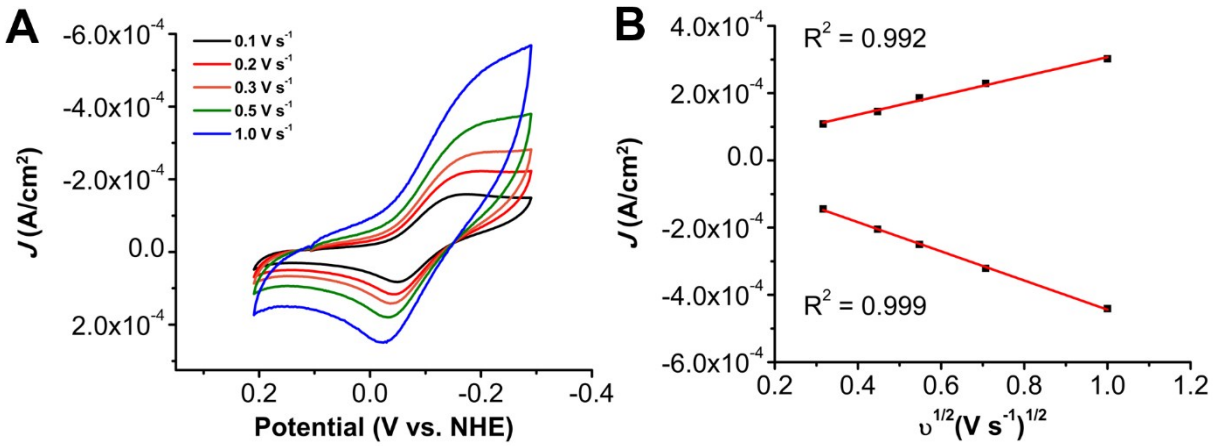

Figure S13. (A) Variable scan rate CVs **(B)** Linear fit demonstrating a homogenous response of $[Mn(TMPyP)Cl]^{4+}$. Conditions: 1 mM $[Mn(TMPyP)Cl]^{+}$ in a pH 14 Britton-Robinson Buffer solution under Ar saturation conditions, glassy carbon working electrode, glassy carbon counter electrode, 3.0 M NaCl Ag/AgCl reference electrode; varied scan rate.

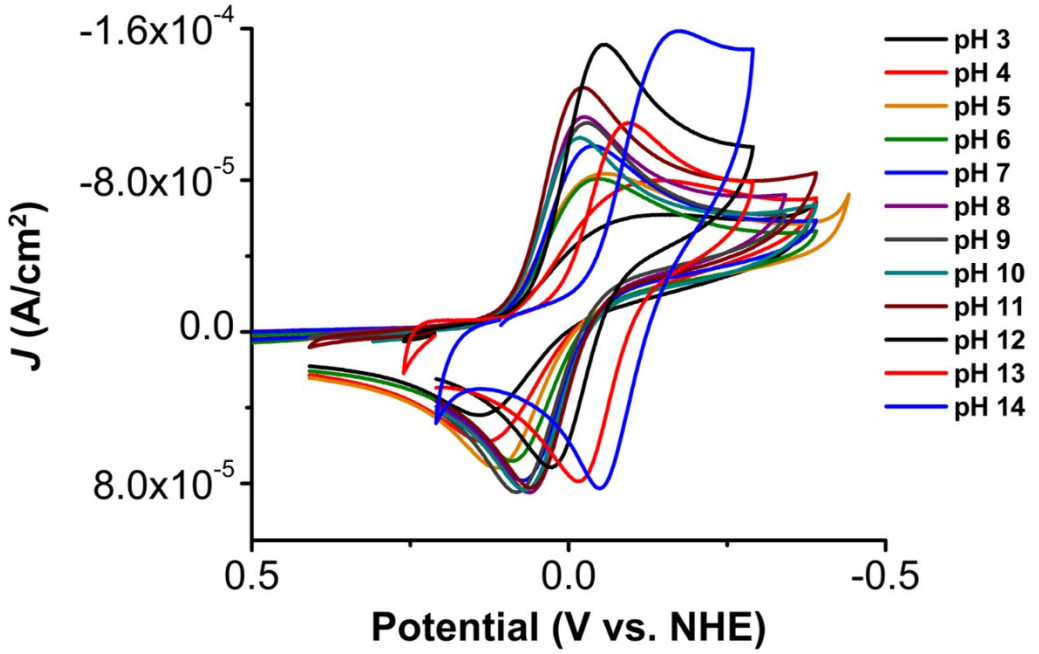

Figure S14. CVs of 1 mM $[Mn(TMPyP)Cl]^{4+}$ demonstrating the shift in $E_{1/2}$ throughout the entire pH domain studied. Ar saturation conditions, glassy carbon working electrode, glassy carbon counter electrode, 3.0 M NaCl Ag/AgCl reference electrode; scan rate 100 mV/s.

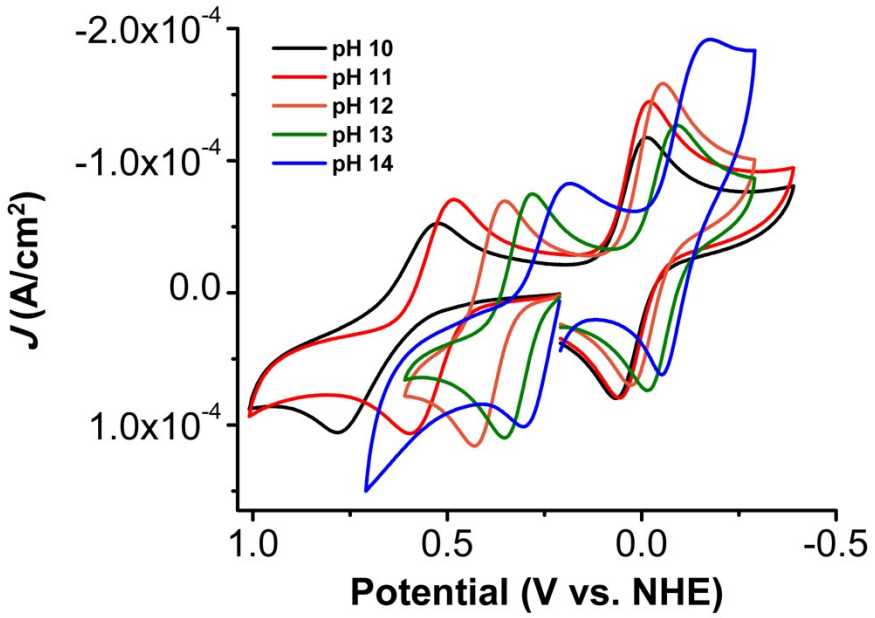

Figure S15. CVs of $[Mn(TMPyP)Cl]^{4+}$ establishing the appearance of a second feature and the pH dependence of the $E_{1/2}$ under basic conditions in a Britton-Robinson buffer. Conditions: 1 mM $[Mn(TMPyP)Cl]^{+}$ in Britton-Robinson Buffer solution at indicated pH under Ar saturation conditions, glassy carbon working electrode, glassy carbon counter electrode, 3.0 M NaCl Ag/AgCl reference electrode; scan rate 100 mV/s.

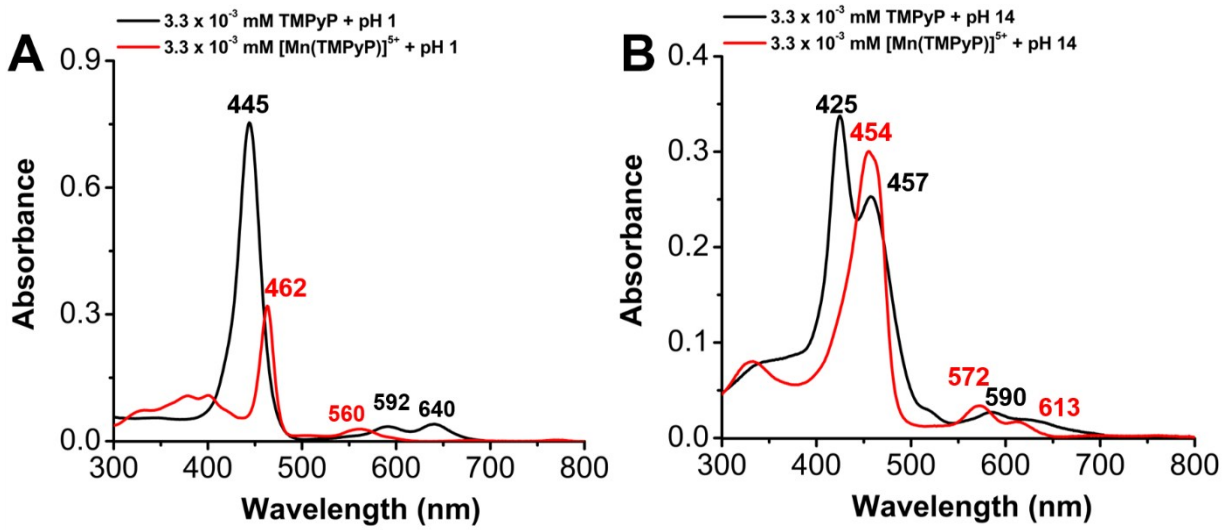

Figure S16. (A) UV-Vis spectrum of $[Mn(TMPyP)Cl]^{4+}$ and free base TMPyP showing that de-metalation does not occur in solution by monitoring the Soret band **(B)** and Q band shifts under pH 1 or 14 conditions.

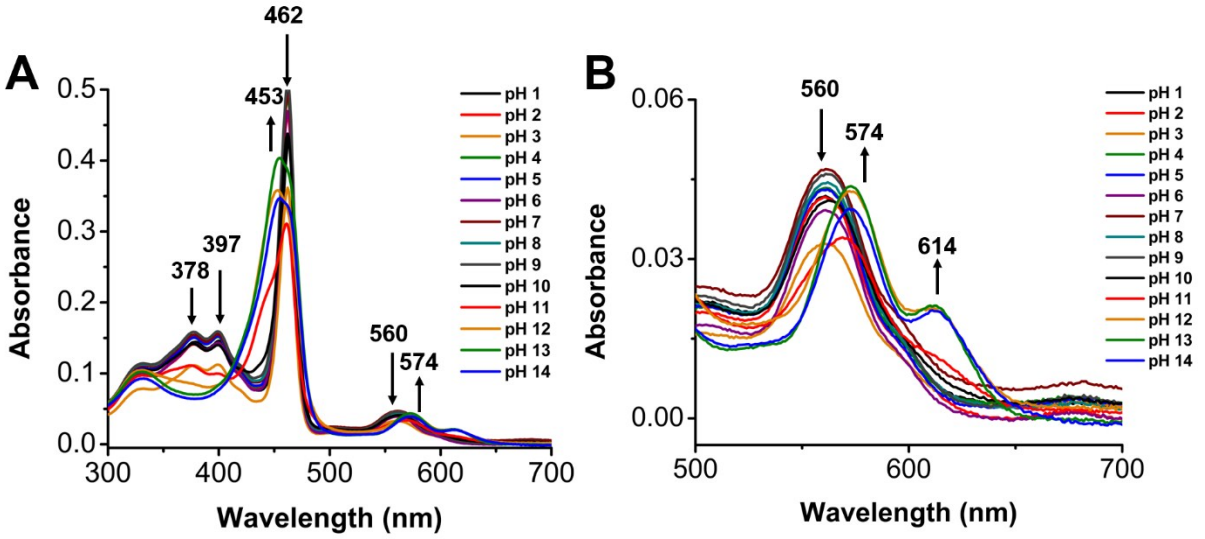

Figure S17. (A) UV-Vis spectrum of 3.33 x 10^{-6} M $[Mn(TMPyP)Cl]^{4+}$ throughout the pH domain with a decrease in absorbance at the characteristic Soret band occurring at 462 nm and the growth of a new band at 453 nm at higher pH **(B)** The characteristic Q band shifting from 560 to 572 towards high pH.

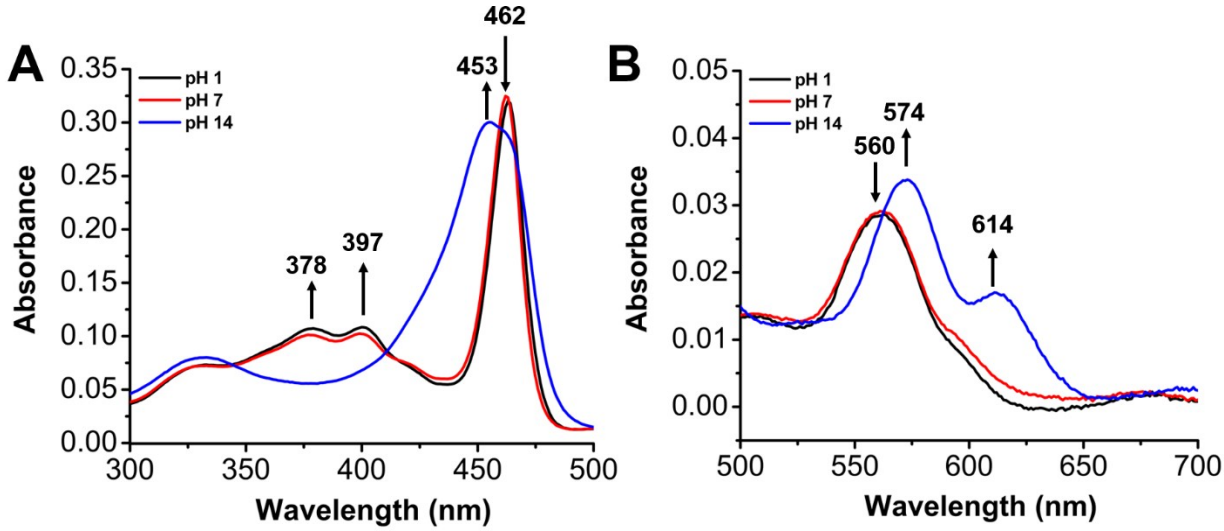

Figure S18. UV-Vis spectrum of 3.33 x 10^{-6} M $[Mn(TMPyP)Cl]^{4+}$ **(A)** Moving to higher pH demonstrates a decrease in absorbance at the Soret band (462 nm) with the appearance of a new band at 453 nm **(B)** While the Q band shifts from 560 to 572 nm.

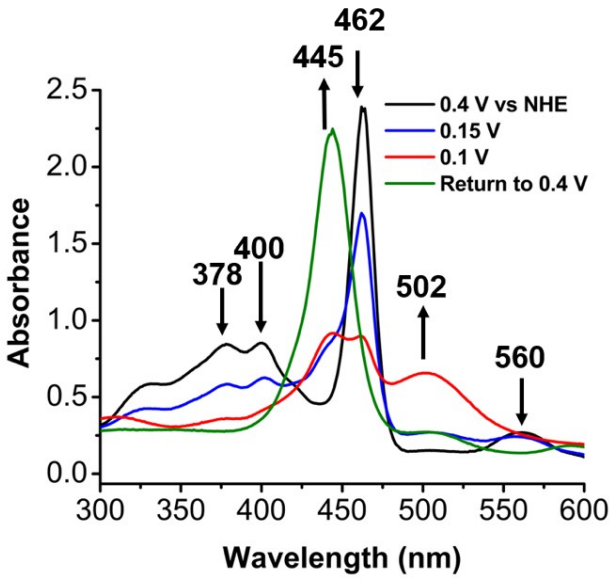

Figure S19. UV-Vis SEC spectrum of 0.1 mM $[Mn(TMPyP)Cl]^{4+}$ at pH 1 showing a decrease in the Soret band at 462 nm with the appearance of a new band at 440 nm as the potential is decreased from +0.40 V to +0.10 V vs NHE. The Q band is blue shifted from 560 to 502 nm upon reduction. Conditions: Honeycomb platinum electrode and Ag/AgCl sat'd KCl aqueous reference electrode.

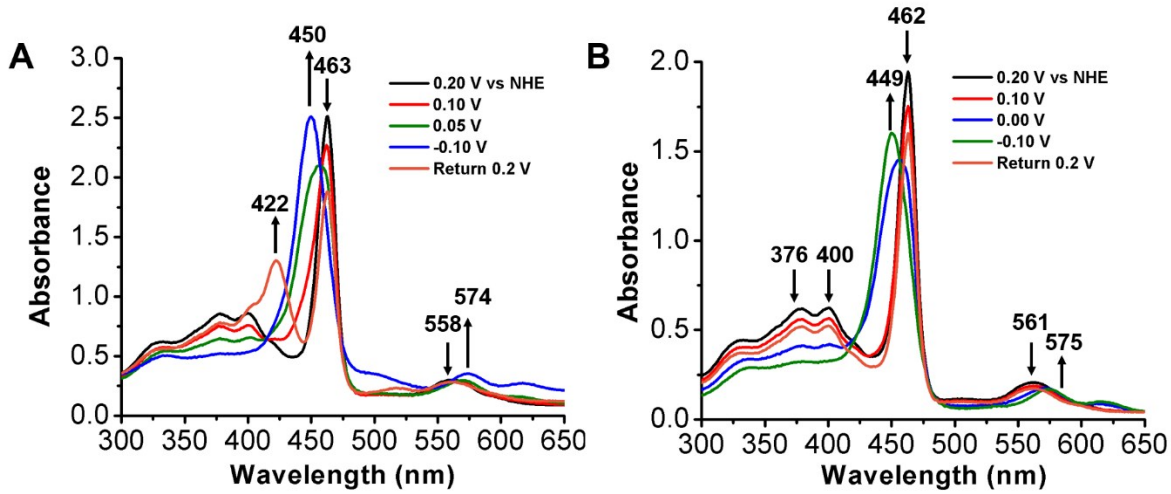

Figure S20. UV-Vis SEC spectra of 0.1 mM $[Mn(TMPyP)Cl]^{4+}$ in **(A)** pH 3 Britton-Robinson buffer solution showing a decrease in the Soret band at 463 nm with the appearance of a new band at 450 nm as the potential is decreased from +0.20 V to –0.10 V vs NHE. The Q band is red shifted from 558 to 574 nm upon reduction. **(B)** pH 7 Britton-Robinson buffer solution showing a decrease in the Soret band at 462 nm with the appearance of a new band at 449 nm as the potential is decreased from +0.20 V to –0.10 V vs NHE. The Q band is red shifted from 561 to 575 nm upon reduction. Conditions: Honeycomb platinum electrode and Ag/AgCl sat'd KCl aqueous reference electrode.

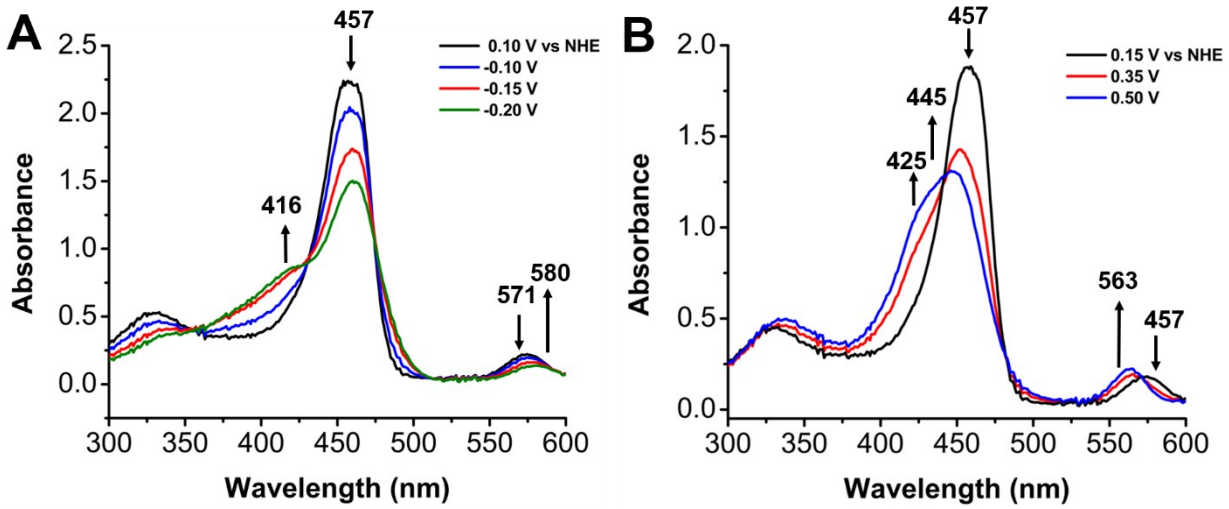

Figure S21. UV-Vis SEC spectrum of 0.1 mM $[Mn(TMPyP)Cl]^{4+}$ in pH 14 Britton-Robinson buffer **(A)** as the potential is decreased from +0.10 V to –0.20 V vs NHE a decrease in the Soret band at 457 nm occurs with the appearance of a new band at 416 nm **(B)** as the potential is increased from +0.15 to +0.50 V vs. NHE the formation of $[Mn(IV)(O)(TMPyP)(OH)]^{3+}$ occurs as apparent from the new band at 425 nm with the loss of the Soret band observed. Conditions: Honeycomb platinum electrode and Ag/AgCl sat'd KCl aqueous reference electrode.

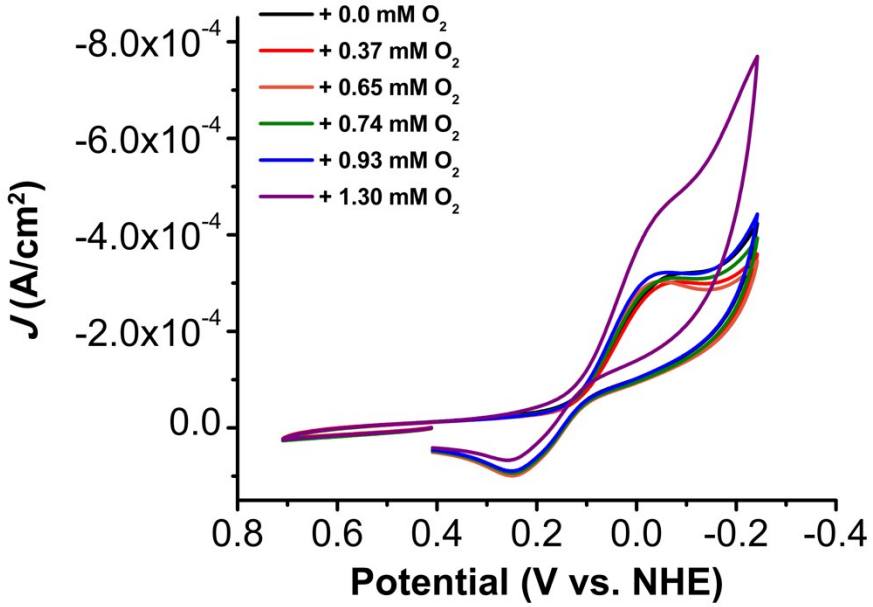

Figure S22. CV of 1 mM $[Mn(TMPyP)Cl]^{4+}$ with O_2 titration showing low activity at pH 1. Conditions: 1 mM $[Mn(TMPyP)Cl]^{4+}$ in a pH 1 (1 M HCl /0.1 M NaCl) solution; glassy carbon working electrode, glassy carbon counter electrode, 3.0 M NaCl Ag/AgCl; scan rate 100 mV/s.

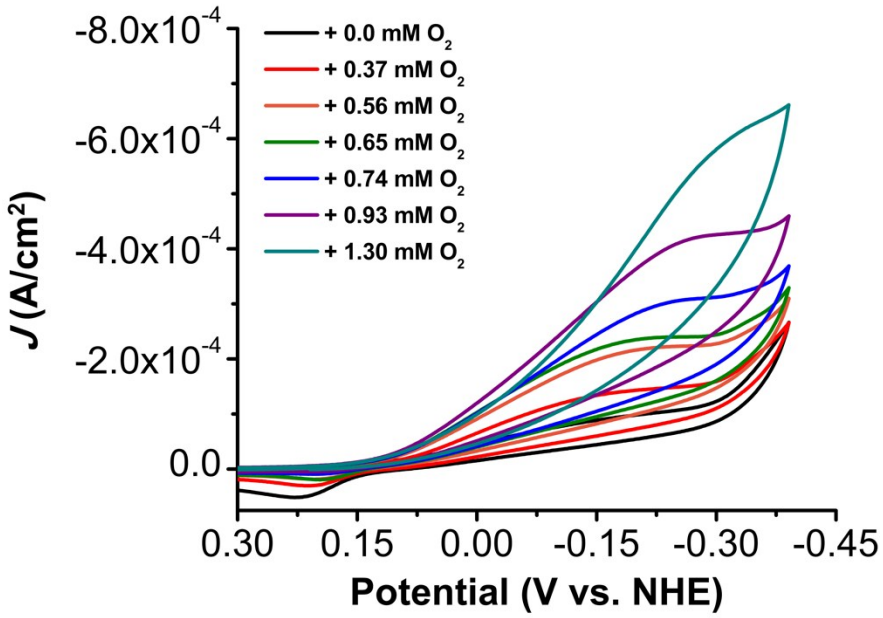

Figure S23. CVs under variable [O_2] showing an irreversible feature under pH 2 Britton-Robinson buffer solution. Conditions: 1 mM $[Mn(TMPyP)Cl]^{4+}$ in a pH 2 Britton-Robinson buffer solution under Ar saturation conditions, glassy carbon working electrode, glassy carbon counter electrode, 3.0 M NaCl Ag/AgCl reference electrode; scan rate 100 mV/s.

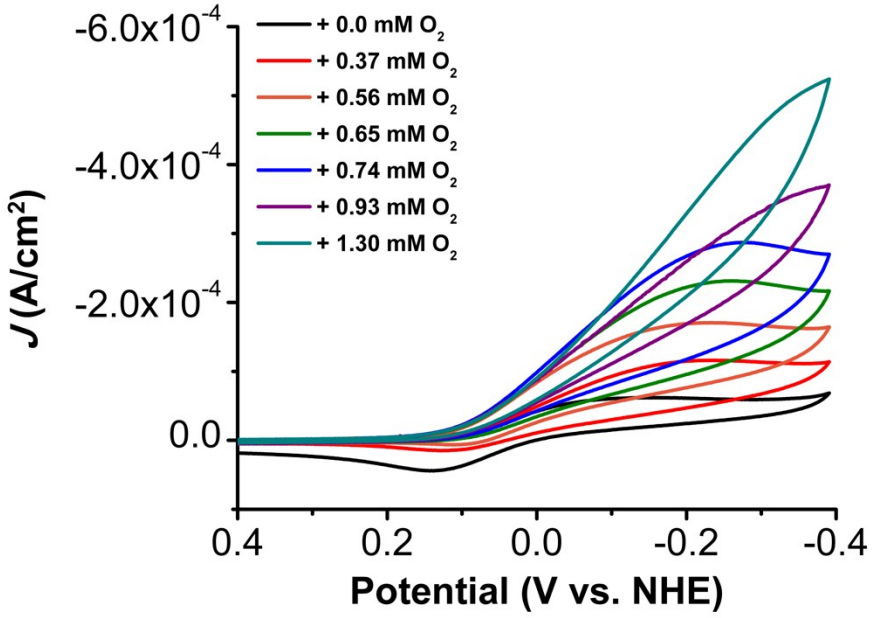

Figure S24. CVs of 1 mM $[Mn(TMPyP)Cl]^{4+}$ with O_2 titration demonstrating catalytic activity. Conditions: 1 mM $[Mn(TMPyP)Cl]^{4+}$ in a pH 3 Britton-Robinson Buffer solution; glassy carbon working electrode, glassy carbon counter electrode, 3.0 M NaCl Ag/AgCl reference electrode; scan rate 100 mV/s.

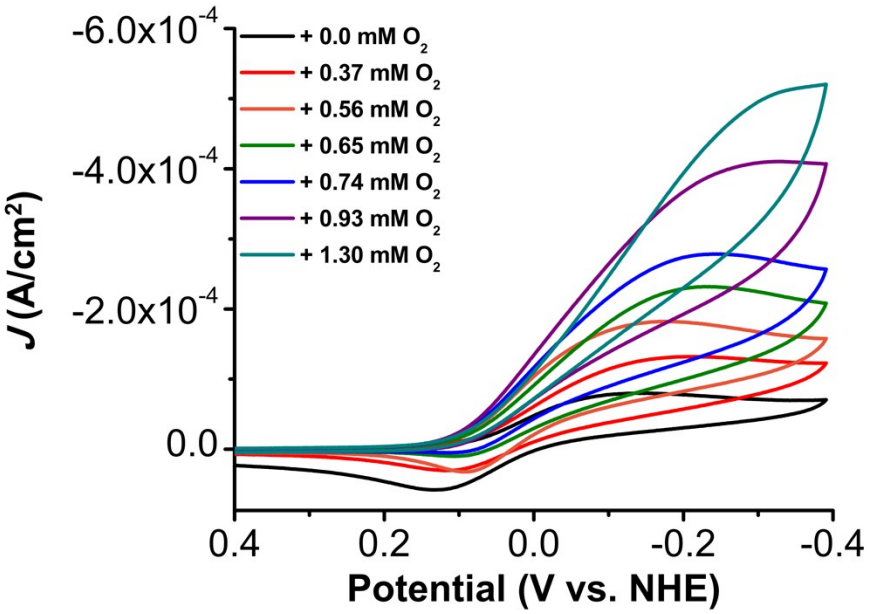

Figure S25. CVs of 1 mM $[Mn(TMPyP)Cl]^{4+}$ with O_2 titration demonstrating catalytic activity. Conditions: 1 mM $[Mn(TMPyP)Cl]^{4+}$ in a pH 4 Britton-Robinson Buffer solution; glassy carbon working electrode, glassy carbon counter electrode, 3.0 M NaCl Ag/AgCl reference; scan rate 100 mV/s.

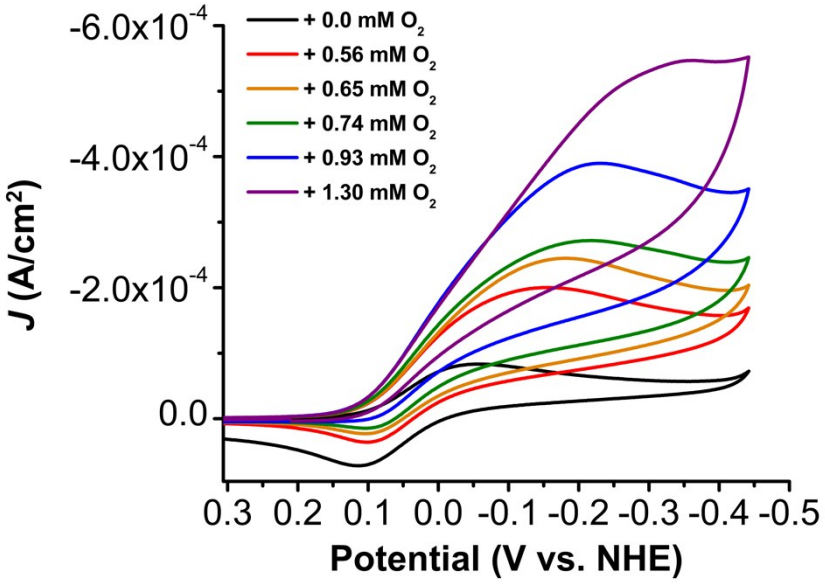

Figure S26. CVs of 1 mM $[Mn(TMPyP)Cl]^{4+}$ with O_2 titration demonstrating catalytic activity. Conditions: 1 mM $[Mn(TMPyP)Cl]^{4+}$ in a pH 5 Britton-Robinson Buffer solution; glassy carbon working electrode, glassy carbon counter electrode, 3.0 M NaCl Ag/AgCl reference; scan rate 100 mV/s.

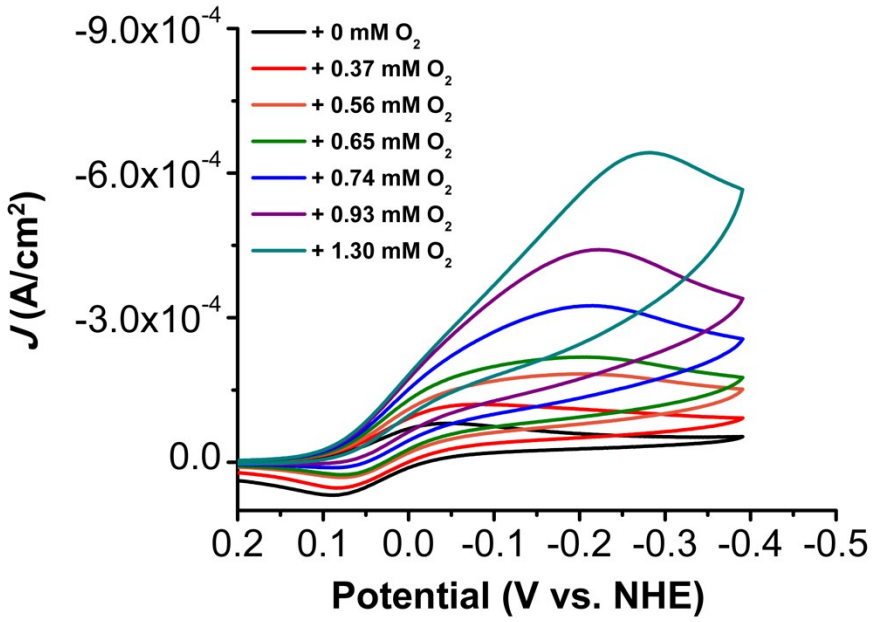

Figure S27. CVs of 1 mM $[Mn(TMPyP)Cl]^{4+}$ with O_2 titration demonstrating catalytic activity. Conditions: 1 mM $[Mn(TMPyP)Cl]^{4+}$ in a pH 6 Britton-Robinson Buffer solution; glassy carbon working electrode, glassy carbon counter electrode, 3.0 M NaCl Ag/AgCl reference; scan rate 100 mV/s.

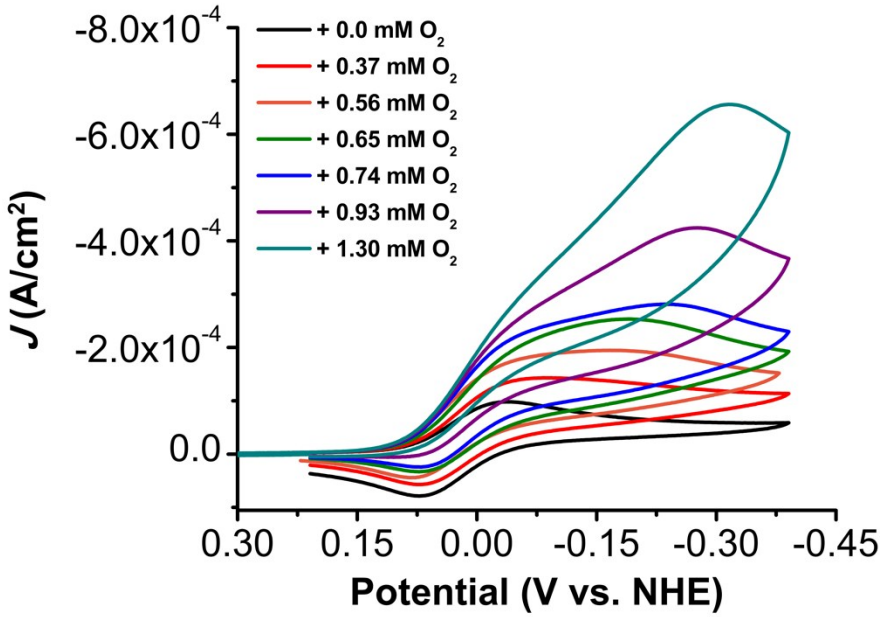

Figure S28. CVs of 1 mM $[Mn(TMPyP)Cl]^{4+}$ with O_2 titration. Conditions: 1 mM $[Mn(TMPyP)Cl]^{4+}$ in a pH 7 Britton-Robinson Buffer solution; glassy carbon working electrode, glassy carbon counter electrode, 3.0 M NaCl Ag/AgCl reference; scan rate 100 mV/s.

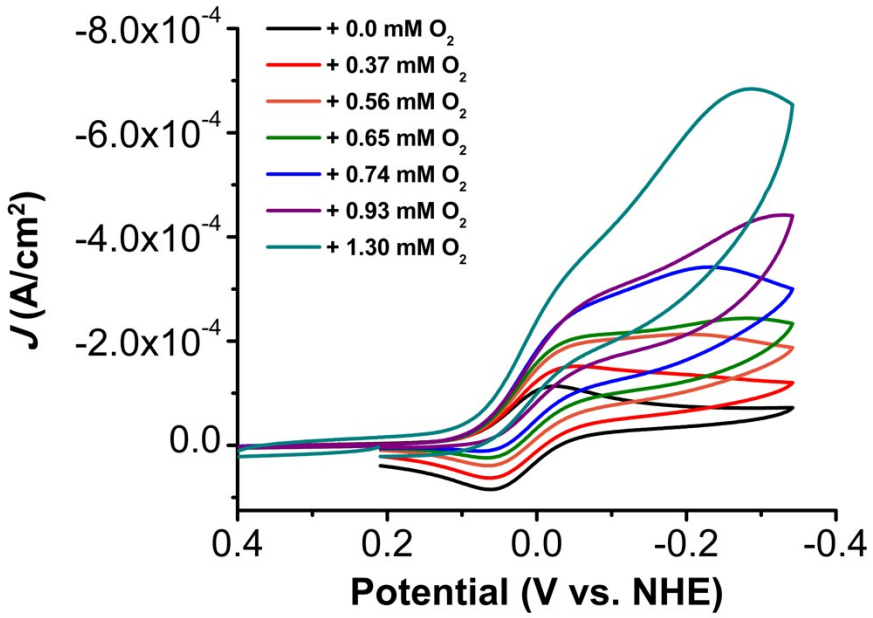

Figure S29. CVs of 1 mM $[Mn(TMPyP)Cl]^{4+}$ with O_2 titration. Conditions: 1 mM $[Mn(TMPyP)Cl]^{4+}$ in a pH 8 Britton-Robinson Buffer solution; glassy carbon working electrode, glassy carbon counter electrode, 3.0 M NaCl Ag/AgCl; scan rate 100 mV/s.

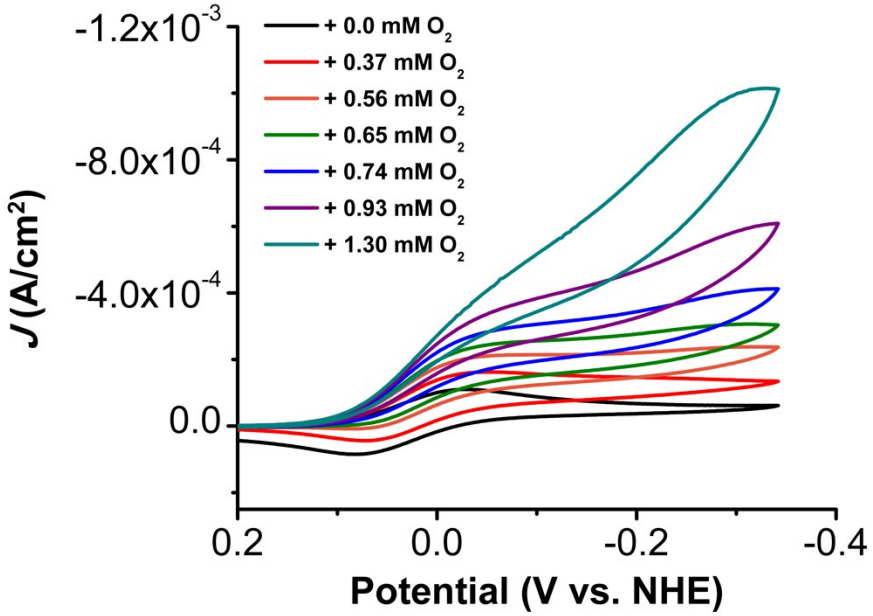

Figure S30. CVs of 1 mM $[Mn(TMPyP)Cl]^{4+}$ with O_2 titration. Conditions: 1 mM $[Mn(TMPyP)Cl]^{4+}$ in a pH 9 Britton-Robinson Buffer solution; glassy carbon working electrode, glassy carbon counter electrode, 3.0 M NaCl Ag/AgCl reference; scan rate 100 mV/s.

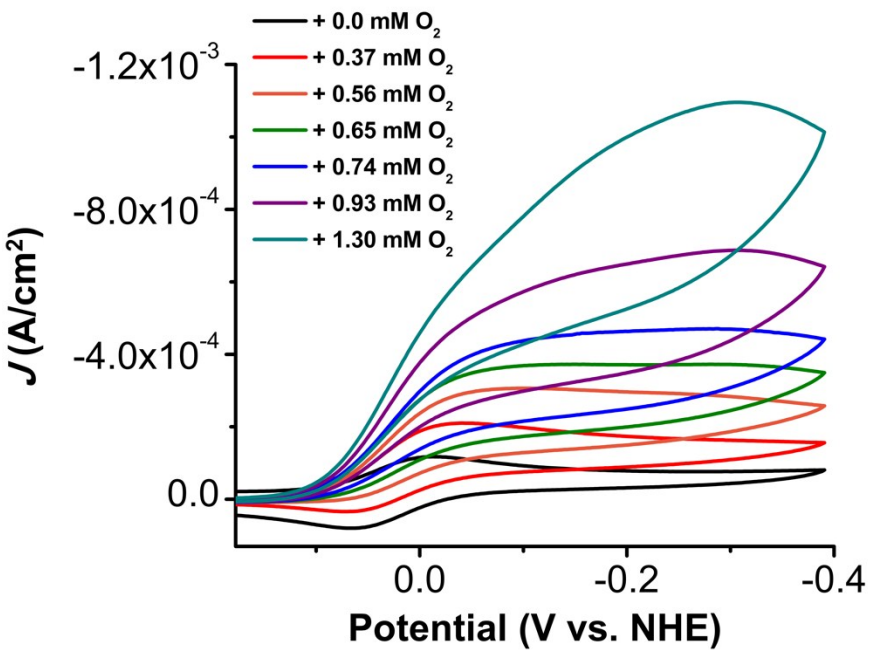

Figure S31. CVs of 1 mM $[Mn(TMPyP)Cl]^{4+}$ with O_2 titration. Conditions: 1 mM $[Mn(TMPyP)Cl]^{4+}$ in a pH 10 Britton-Robinson Buffer solution; glassy carbon working electrode, glassy carbon counter electrode, 3.0 M NaCl Ag/AgCl reference; scan rate 100 mV/s.

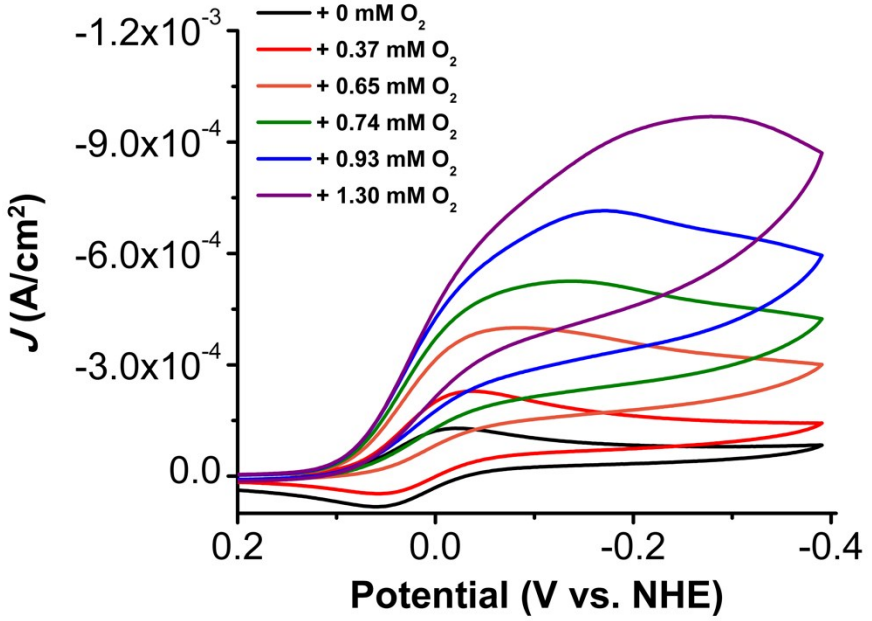

Figure S32. CVs of 1 mM $[Mn(TMPyP)Cl]^{4+}$ with O_2 titration. Conditions: 1 mM $[Mn(TMPyP)Cl]^{4+}$ in a pH 11 Britton-Robinson Buffer solution; glassy carbon working electrode, glassy carbon counter electrode, 3.0 M NaCl Ag/AgCl reference; scan rate 100 mV/s.

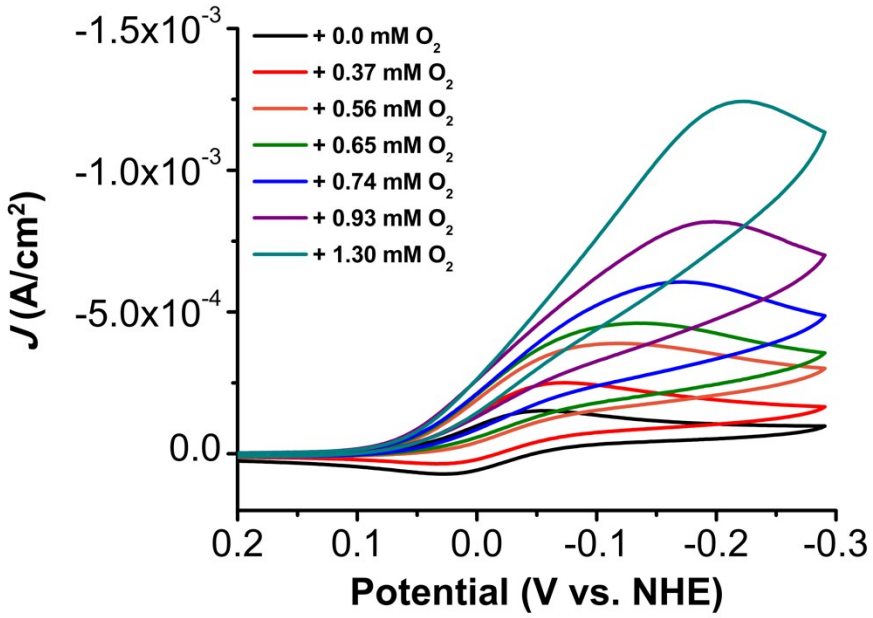

Figure S33. CVs of 1 mM $[Mn(TMPyP)Cl]^{4+}$ with O_2 titration. Conditions: 1 mM $[Mn(TMPyP)Cl]^{4+}$ in a pH 12 Britton-Robinson Buffer solution; glassy carbon working electrode, glassy carbon counter electrode, 3.0 M NaCl Ag/AgCl reference; scan rate 100 mV/s.

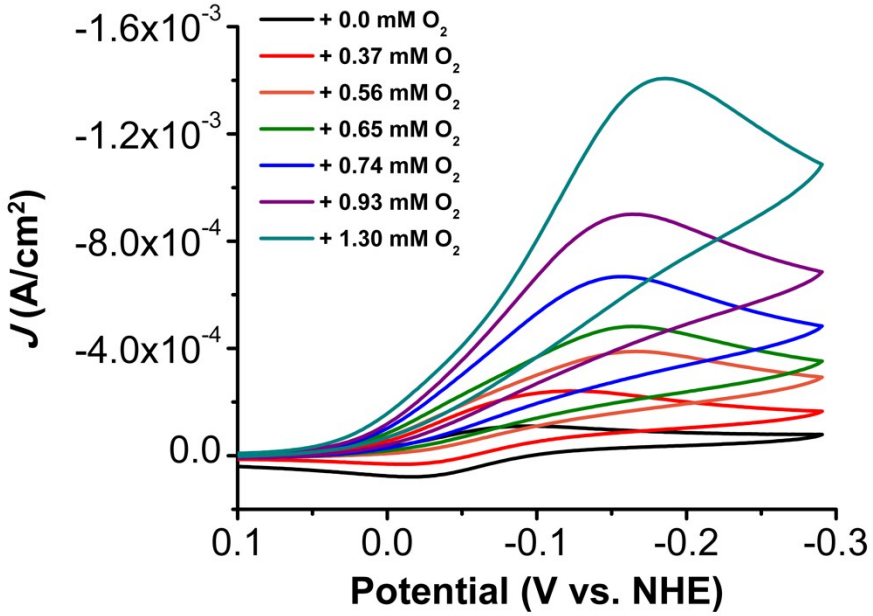

Figure S34. CVs of 1 mM $[Mn(TMPyP)Cl]^{4+}$ with O_2 titration. Conditions: 1 mM $[Mn(TMPyP)Cl]^{4+}$ in a pH 13 Britton-Robinson Buffer solution; glassy carbon working electrode, glassy carbon counter electrode, 3.0 M NaCl Ag/AgCl reference; scan rate 100 mV/s.

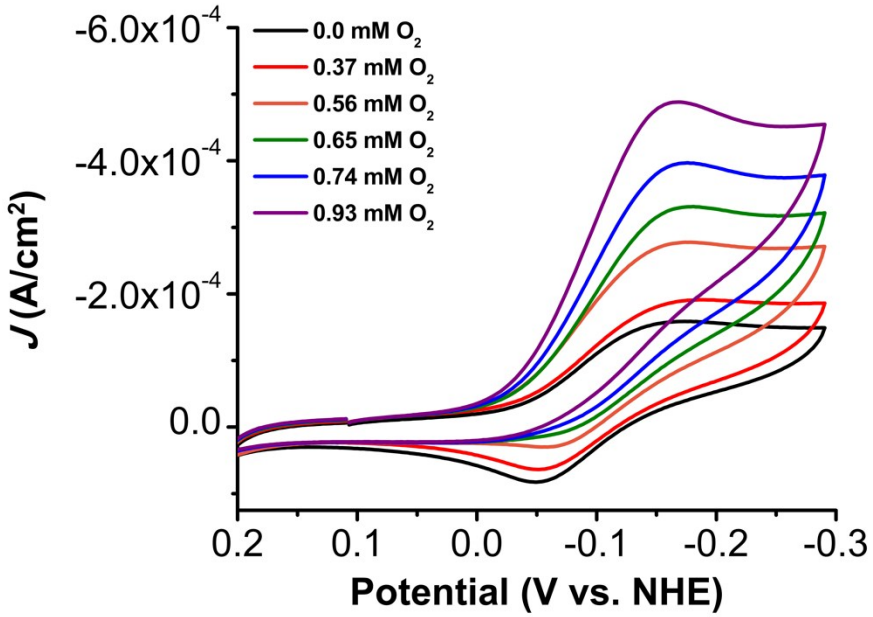

Figure S35. CVs of 1 mM $[Mn(TMPyP)Cl]^{4+}$ with O_2 titration. Conditions: 1 mM $[Mn(TMPyP)Cl]^{4+}$ in a pH 14 Britton-Robinson Buffer solution; glassy carbon working electrode, glassy carbon counter electrode, 3.0 M NaCl Ag/AgCl reference; scan rate 100 mV/s.

Cyclic Voltammetry Controls

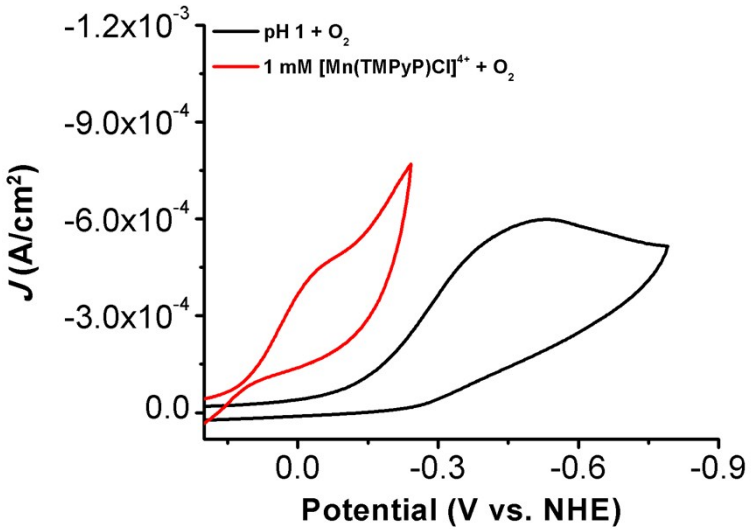

Figure S36. Control CV of a blank pH 1 (1 M HCl / 0.1 M NaCl) solution under O_2 saturation conditions in comparison to a 1 mM $[Mn(TMPyP)Cl]^{4+}$ solution under O_2 showing the molecular regime for the catalyst. Conditions: Glassy carbon working electrode, glassy carbon counter electrode, 3.0 M NaCl Ag/AgCl reference electrode; scan rate 100 mV/s.

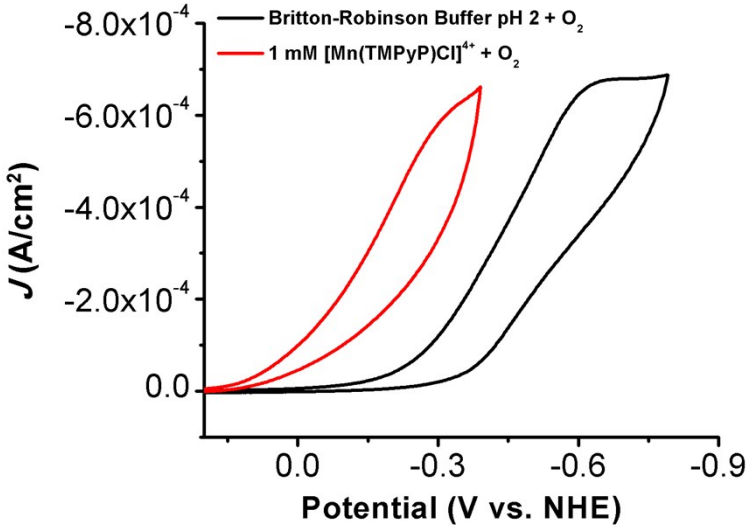

Figure S37. Control CV of a blank pH 2 Britton-Robinson Buffer solution under O_2 saturation conditions in comparison to a 1 mM $[Mn(TMPyP)Cl]^{4+}$ solution under O_2 showing the molecular regime for the catalyst. Conditions: Glassy carbon working electrode, glassy carbon counter electrode, 3.0 M NaCl Ag/AgCl reference electrode; scan rate 100 mV/s.

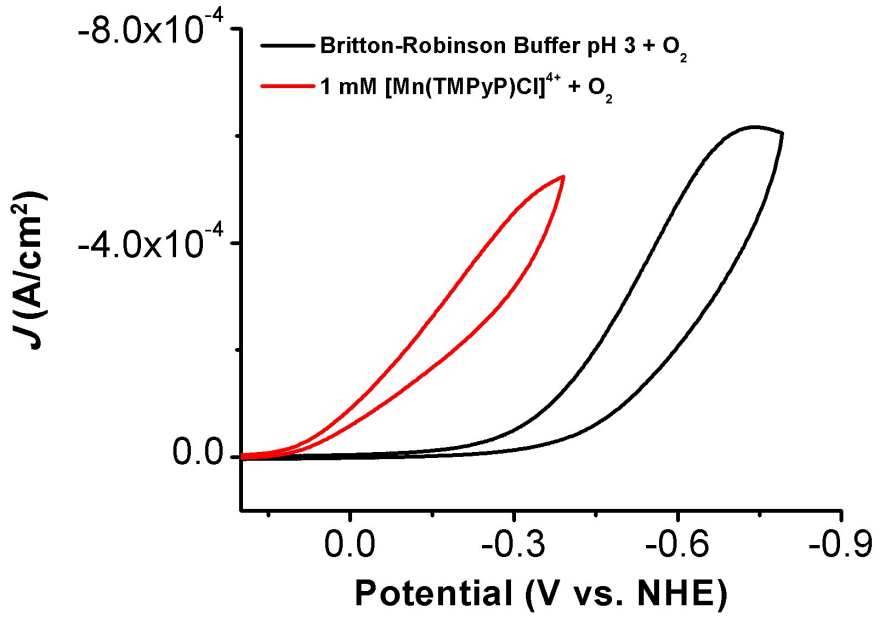

Figure S38. Control CV of a blank pH 3 Britton-Robinson Buffer solution under O_2 saturation conditions in comparison to a 1 mM $[Mn(TMPyP)Cl]^{4+}$ solution under O_2 showing the molecular regime for the catalyst. Conditions: Glassy carbon working electrode, glassy carbon counter electrode, 3.0 M NaCl Ag/AgCl reference electrode; scan rate 100 mV/s.

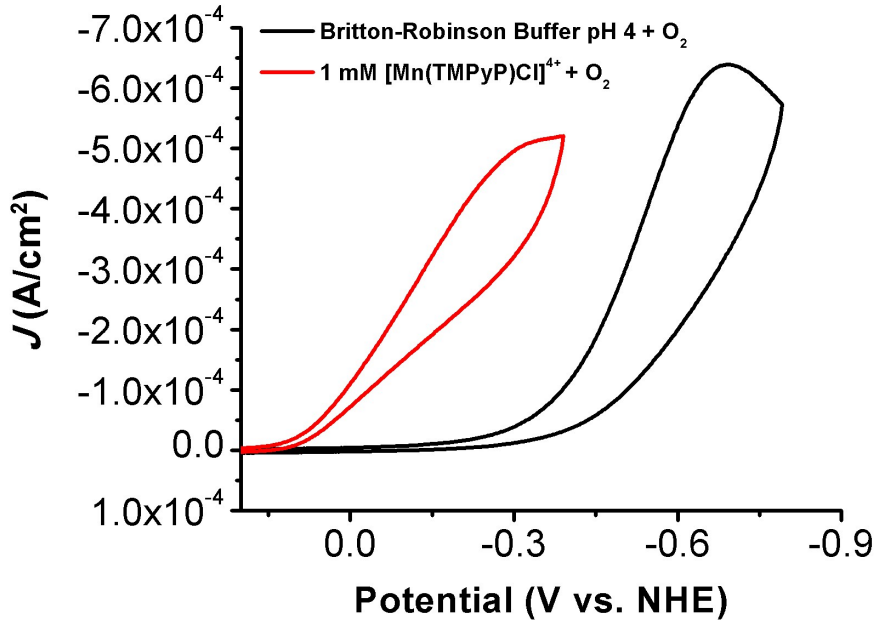

Figure S39. Control CV of a blank pH 4 Britton-Robinson Buffer solution under O_2 saturation conditions in comparison to a 1 mM $[Mn(TMPyP)Cl]^{4+}$ solution under O_2 showing the molecular regime for the catalyst. Conditions: Glassy carbon working electrode, glassy carbon counter electrode, 3.0 M NaCl Ag/AgCl reference electrode; scan rate 100 mV/s.

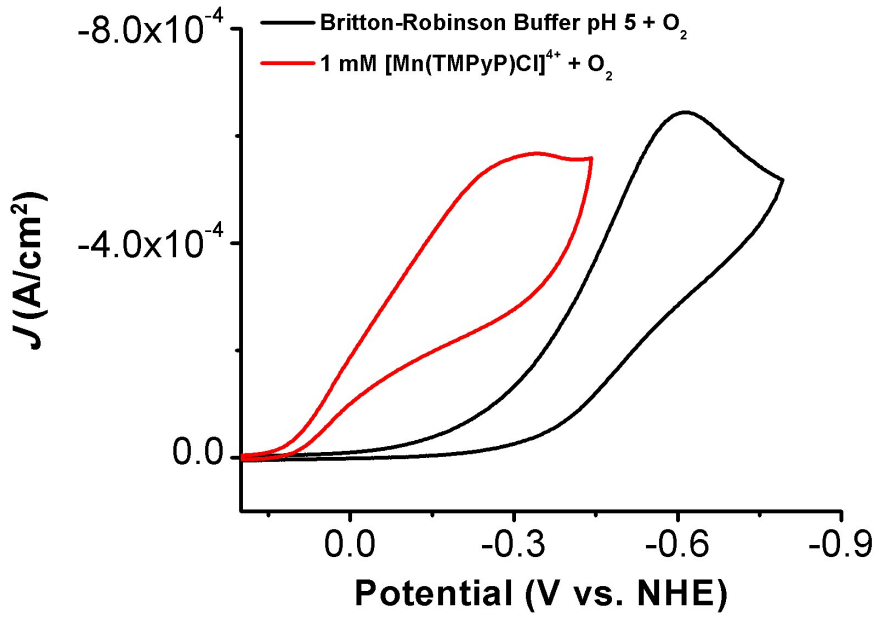

Figure S40. Control CV of a blank pH 5 Britton-Robinson Buffer solution under O_2 saturation conditions in comparison to a 1 mM $[Mn(TMPyP)Cl]^{4+}$ solution under O_2 showing the molecular regime for the catalyst. Conditions: Glassy carbon working electrode, glassy carbon counter electrode, 3.0 M NaCl Ag/AgCl reference electrode; scan rate 100 mV/s.

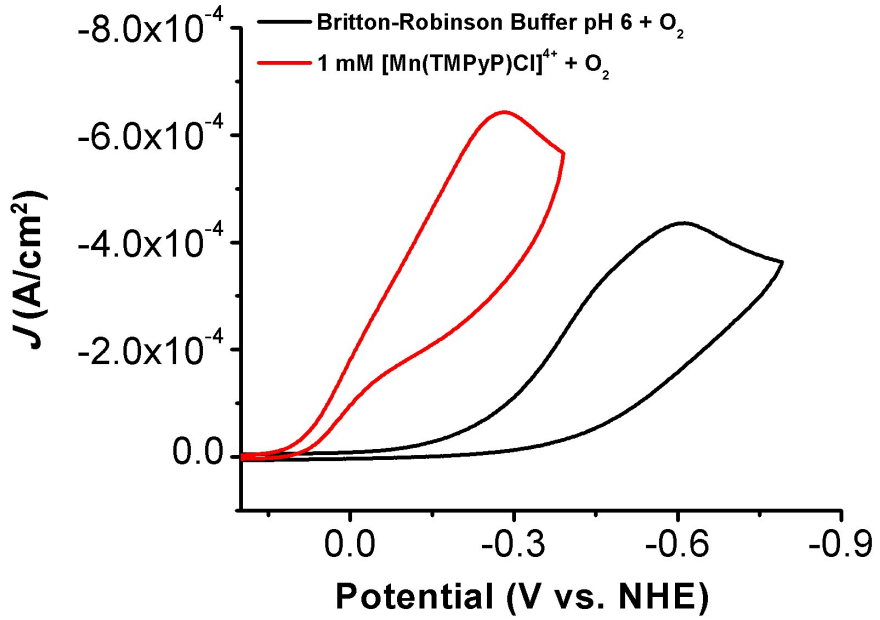

Figure S41. Control CV of a blank pH 6 Britton-Robinson Buffer solution under O_2 saturation conditions in comparison to a 1 mM $[Mn(TMPyPCl)]^{4+}$ solution under O_2 showing the molecular regime for the catalyst. Conditions: Glassy carbon working electrode, glassy carbon counter electrode, 3.0 M NaCl Ag/AgCl reference electrode; scan rate 100 mV/s.

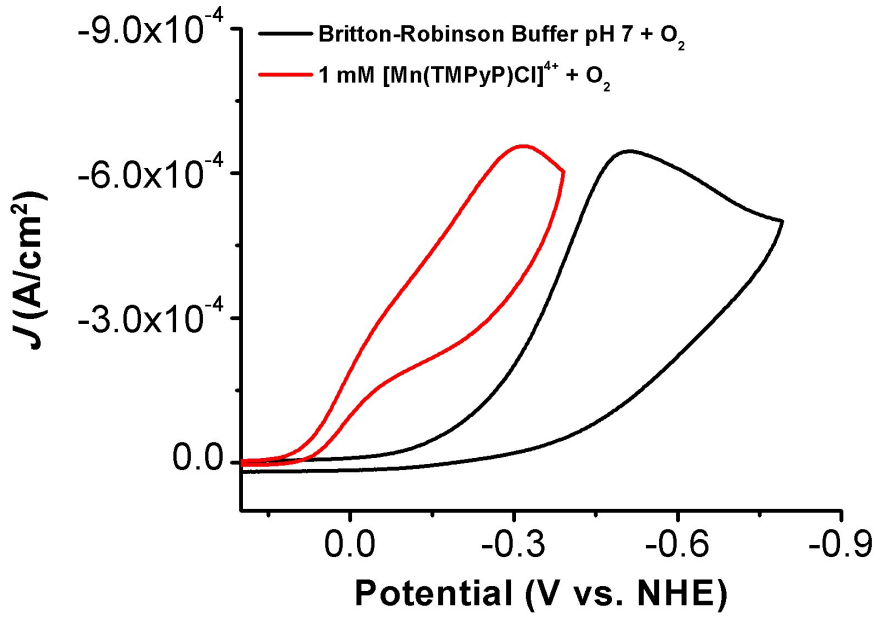

Figure S42. Control CV of a blank pH 7 Britton-Robinson Buffer solution under O_2 saturation conditions in comparison to a 1 mM $[Mn(TMPyP)Cl]^{4+}$ solution under O_2 showing the molecular regime for the catalyst. Conditions: Glassy carbon working electrode, glassy carbon counter electrode, 3.0 M NaCl Ag/AgCl reference electrode; scan rate 100 mV/s.

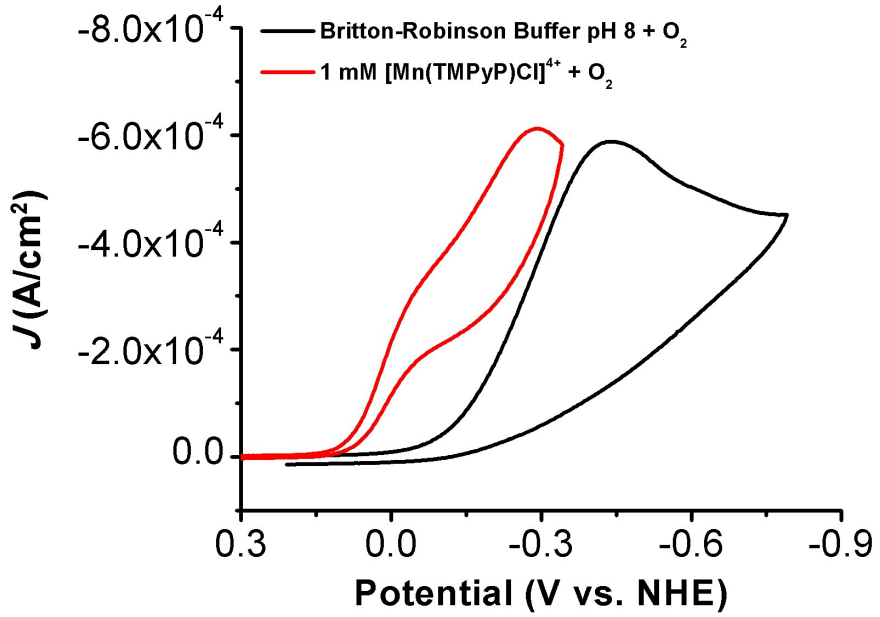

Figure S43. Control CV of a blank pH 8 Britton-Robinson Buffer solution under O_2 saturation conditions in comparison to a 1 mM $[Mn(TMPyP)Cl]^{4+}$ solution under O_2 showing the molecular regime for the catalyst. Conditions: Glassy carbon working electrode, glassy carbon counter electrode, 3.0 M NaCl Ag/AgCl reference; scan rate 100 mV/s.

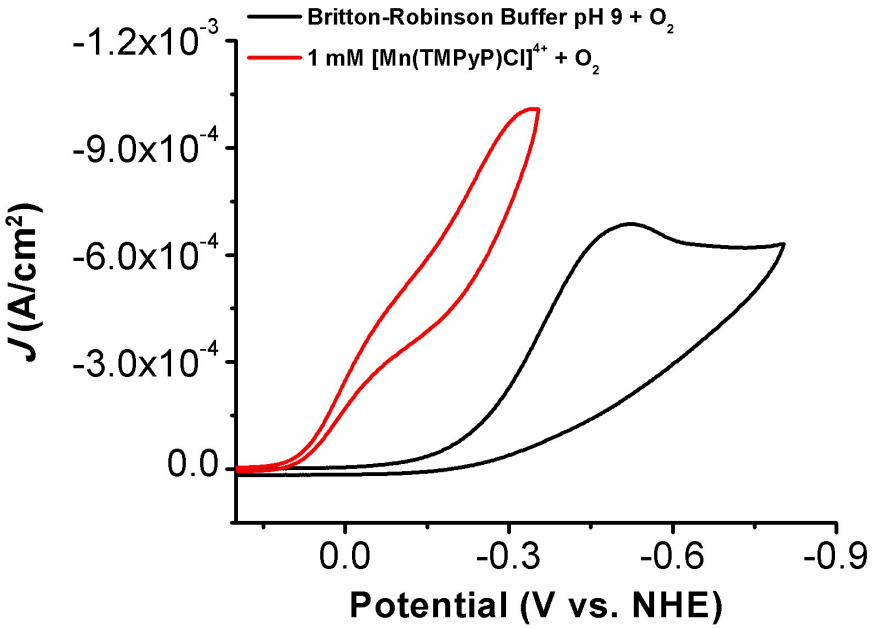

Figure S44. Control CV of a blank pH 9 Britton-Robinson Buffer solution under O_2 saturation conditions in comparison to a 1 mM $[Mn(TMPyP)Cl]^{4+}$ solution under O_2 showing the molecular regime for the catalyst. Conditions: Glassy carbon working electrode, glassy carbon counter electrode, 3.0 M NaCl Ag/AgCl reference electrode; scan rate 100 mV/s.

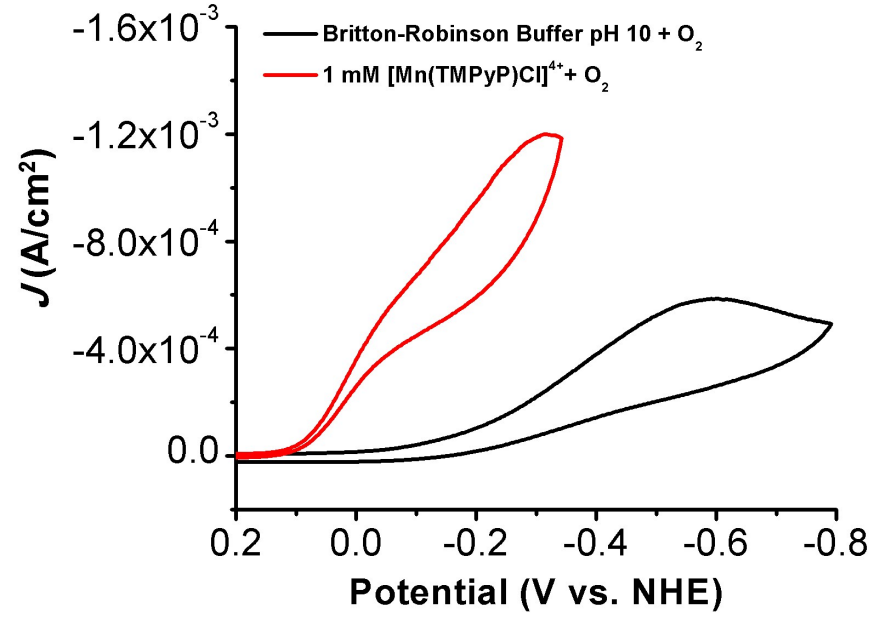

Figure S45. Control CV of a blank pH 10 Britton-Robinson Buffer solution under O_2 saturation conditions in comparison to a 1 mM $[Mn(TMPyP)Cl]^{4+}$ solution under O_2 showing the molecular regime for the catalyst. Conditions: Glassy carbon working electrode, glassy carbon counter electrode, 3.0 M NaCl Ag/AgCl reference electrode; scan rate 100 mV/s.

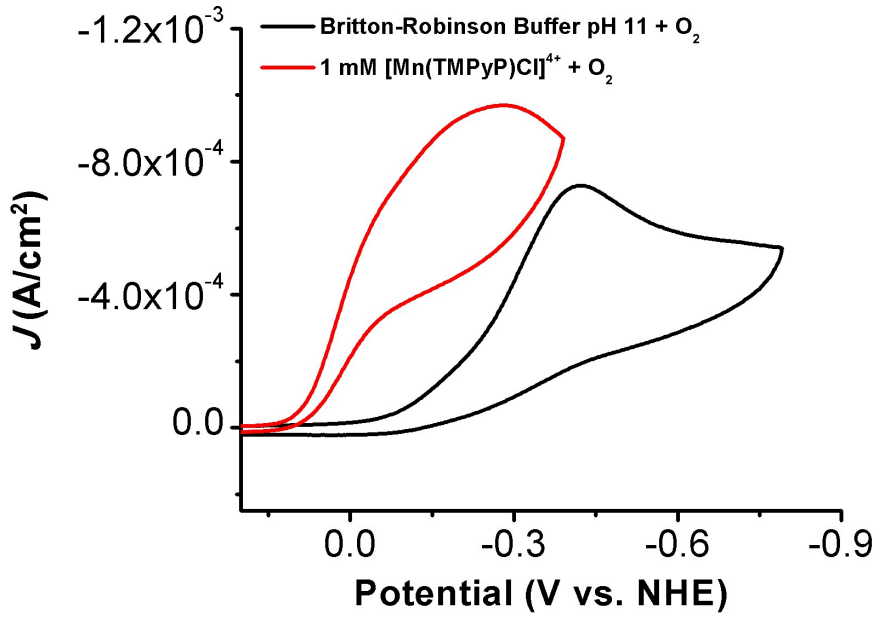

Figure S46. Control CV of a blank pH 11 Britton-Robinson Buffer solution under O_2 saturation conditions in comparison to a 1 mM $[Mn(TMPyP)Cl]^{4+}$ solution under O_2 showing the molecular regime for the catalyst. Conditions: Glassy carbon working electrode, glassy carbon counter electrode, 3.0 M NaCl Ag/AgCl reference electrode; scan rate 100 mV/s.

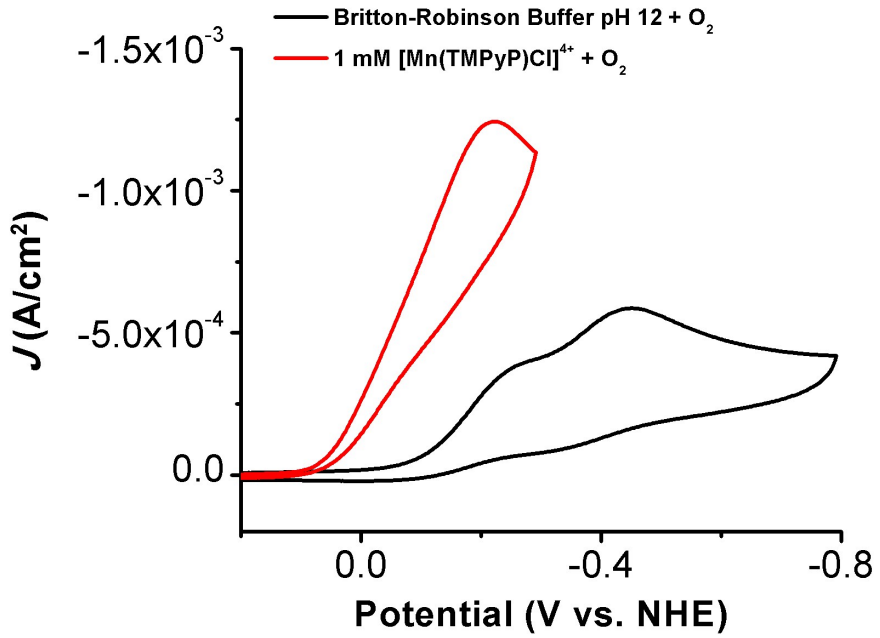

Figure S47. Control CV of a blank pH 12 Britton-Robinson Buffer solution under O_2 saturation conditions in comparison to a 1 mM $[Mn(TMPyP)Cl]^{4+}$ solution under O_2 showing the molecular regime for the catalyst. Conditions: Glassy carbon working electrode, glassy carbon counter electrode, 3.0 M NaCl Ag/AgCl reference electrode; scan rate 100 mV/s.

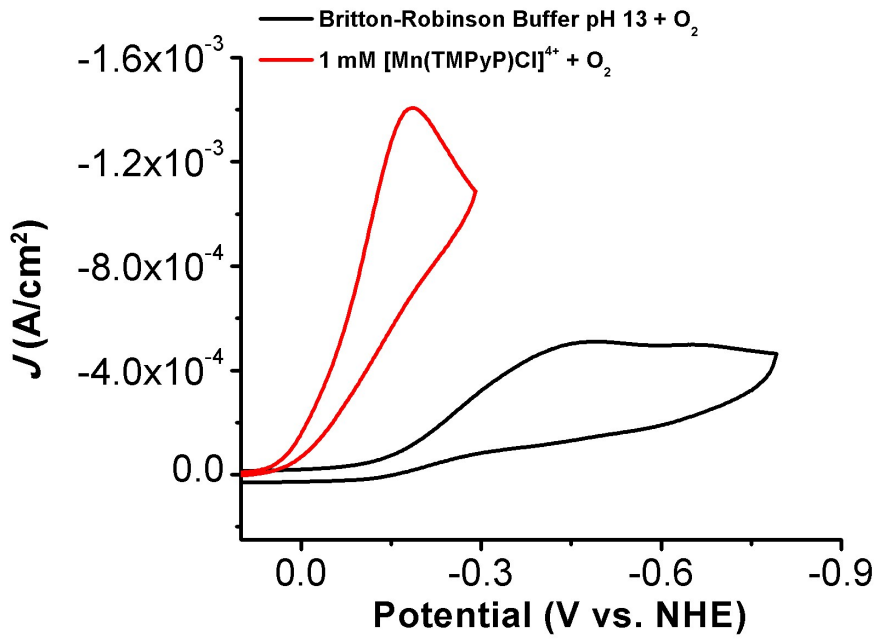

Figure S48. Control CV of a blank pH 13 Britton-Robinson Buffer solution under O_2 saturation conditions in comparison to a 1 mM $[Mn(TMPyP)Cl]^{4+}$ solution under O_2 showing the molecular regime for the catalyst. Conditions: Glassy carbon working electrode, glassy carbon counter electrode, 3.0 M NaCl Ag/AgCl reference electrode; scan rate 100 mV/s.

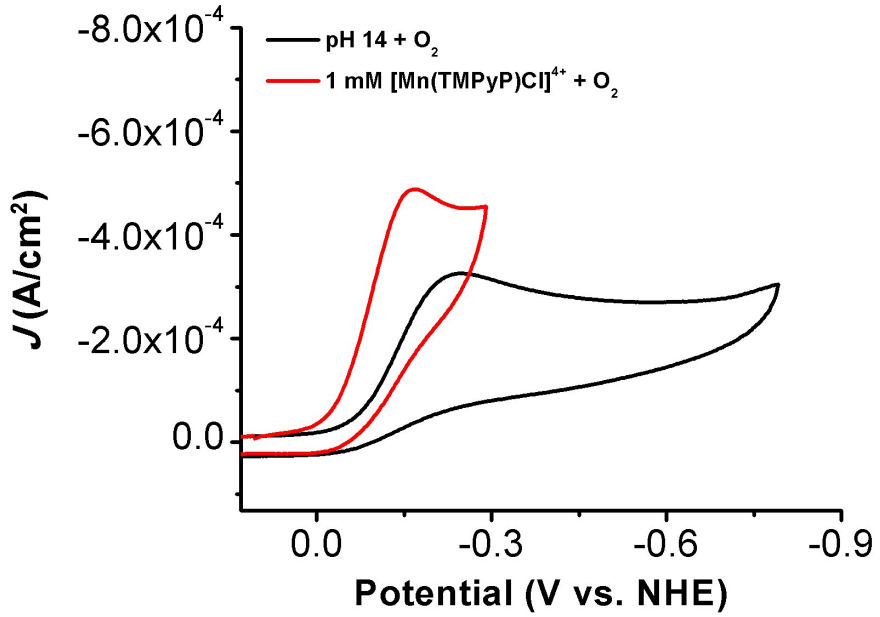

Figure S49. Control CV of a blank pH 14 (1 M KOH / 0.1 M NaCl) solution under O_2 saturation conditions in comparison to a 1 mM $[Mn(TMPyP)Cl]^{4+}$ solution under O_2 showing the molecular regime for the catalyst. Conditions: Glassy carbon working electrode, glassy carbon counter electrode, 3.0 M NaCl Ag/AgCl reference electrode; scan rate 100 mV/s.

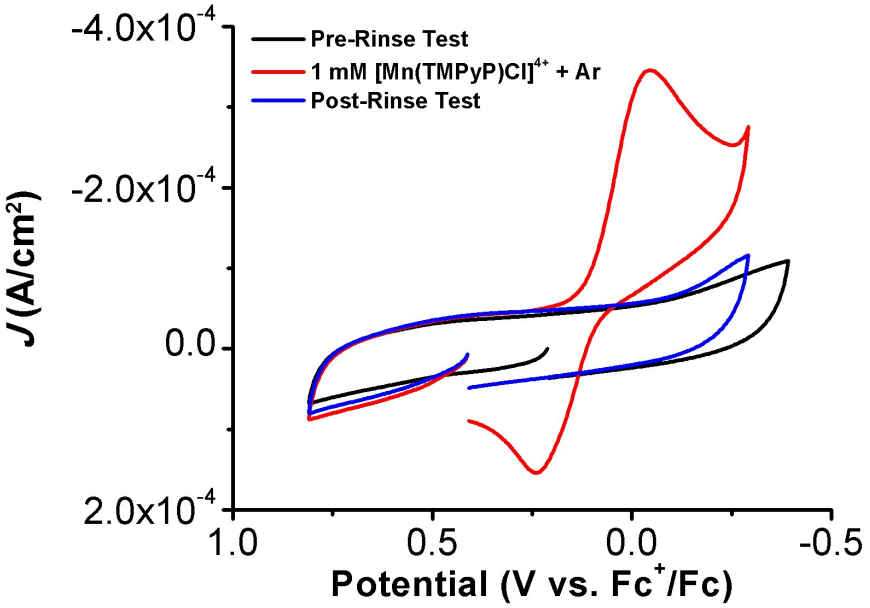

Figure S50. Rinse test at pH 1 (1 M HCl / 0.1 M NaCl) solution under Ar. Conditions: Glassy carbon working electrode, glassy carbon counter electrode, 3.0 M NaCl Ag/AgCl reference electrode; scan rate 100 mV/s.

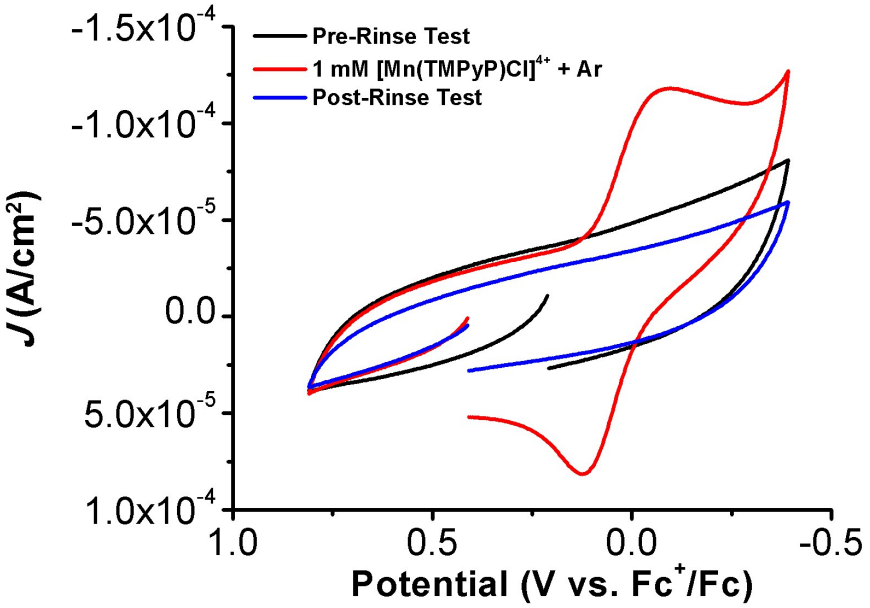

Figure S51. Rinse test at pH 3 Britton-Robinson Buffer solution under Ar. Conditions: Glassy carbon working electrode, glassy carbon counter electrode, 3.0 M NaCl Ag/AgCl reference electrode; scan rate 100 mV/s.

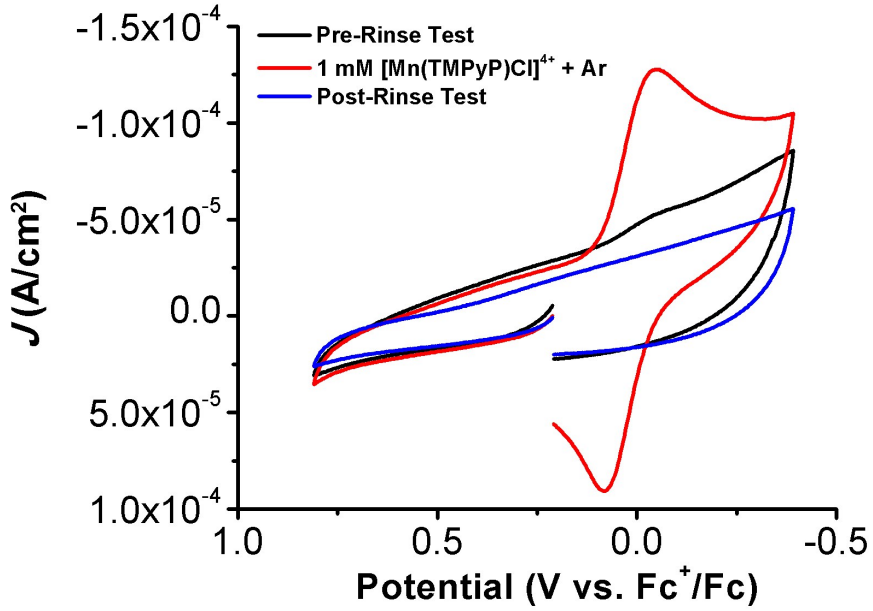

Figure S52. Rinse test at pH 6 Britton-Robinson Buffer solution under Ar. Conditions: Glassy carbon working electrode, glassy carbon counter electrode, 3.0 M NaCl Ag/AgCl reference electrode; scan rate 100 mV/s.

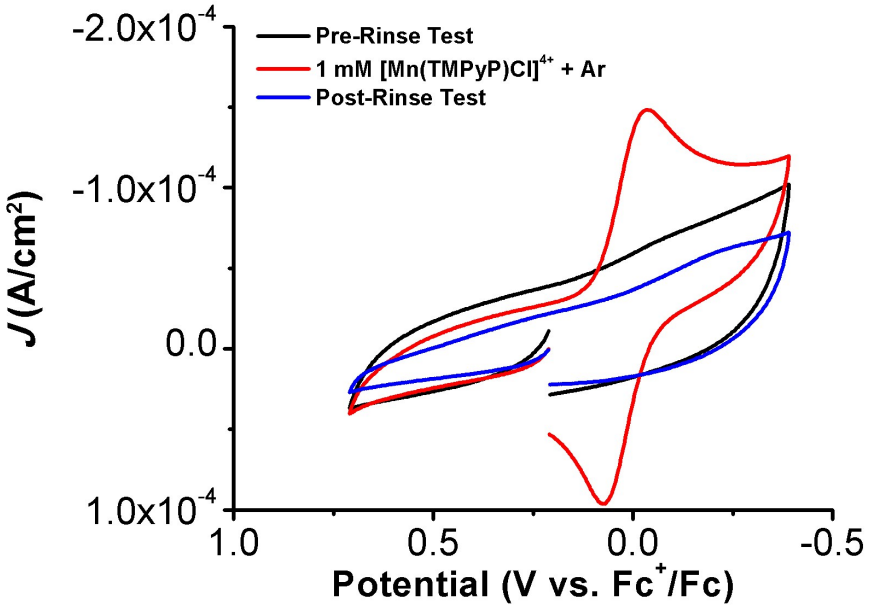

Figure S53. Rinse test at pH 7 Britton-Robinson Buffer solution under Ar. Conditions: Glassy carbon working electrode, glassy carbon counter electrode, 3.0 M NaCl Ag/AgCl reference electrode; scan rate 100 mV/s.

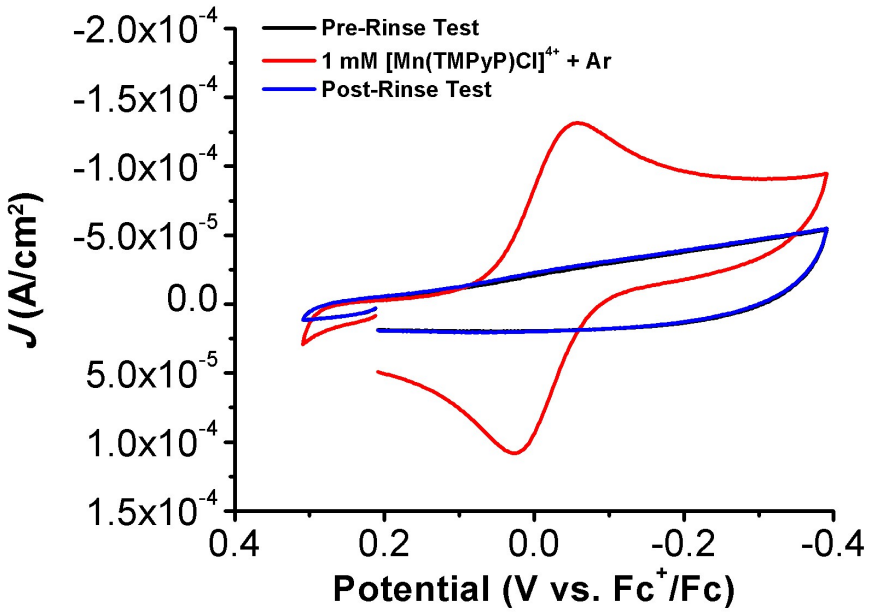

Figure S54. Rinse test at pH 12 Britton-Robinson Buffer solution under Ar. Conditions: Glassy carbon working electrode, glassy carbon counter electrode, 3.0 M NaCl Ag/AgCl reference electrode; scan rate 100 mV/s.

Rotating Ring Disc Electrode (RRDE) Analysis

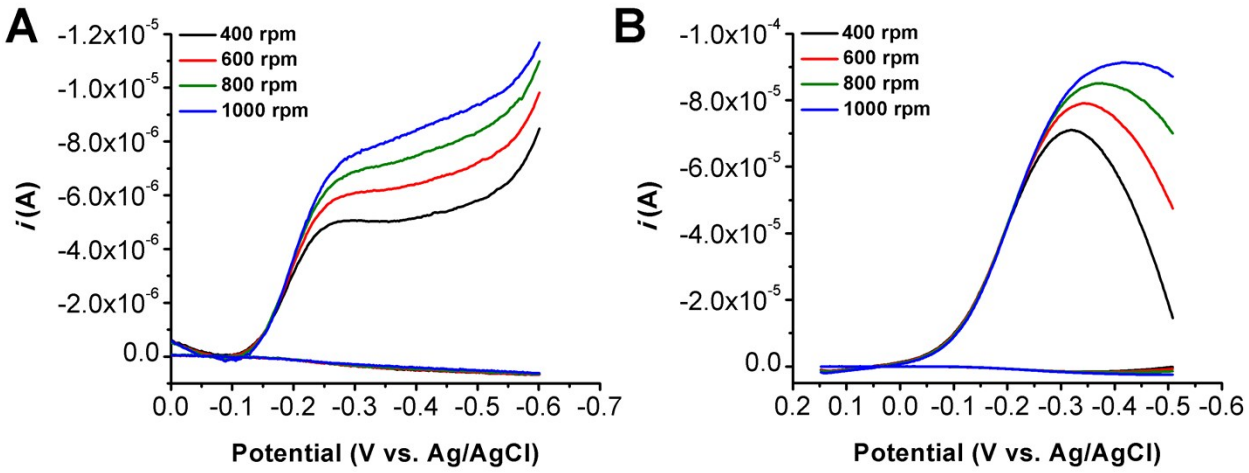

Figure S55. Linear Sweep Voltammograms of RRDE experiments with $[Mn(TMPyP)Cl]^{4+}$ (0.25 mM) at various rotation rates under argon **(A)** and O_2 **(B)** saturation conditions in a pH 5 buffer solution; ring potential = 1.2 V vs Ag/AgCl. Conditions: 0.25 mM analyte; glassy carbon working electrode/Pt ring working electrode, glassy carbon counter electrode, Ag/AgCl/3 M KCl reference electrode; scan rate 0.02 V/s.

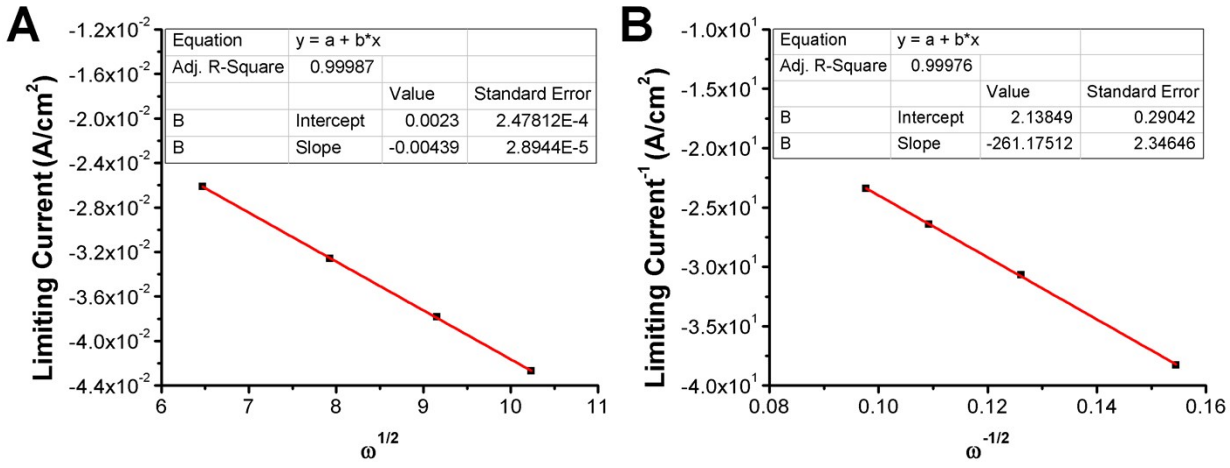

Figure S56. Levich **(A)** and Koutecky-Levich **(B)** plots from data obtained from Linear Sweep Voltammograms of $[Mn(TMPyP)Cl]^{4+}$ (0.25 mM) by RRDE under argon saturation conditions at various rotation rates in a pH 5 buffer solution.

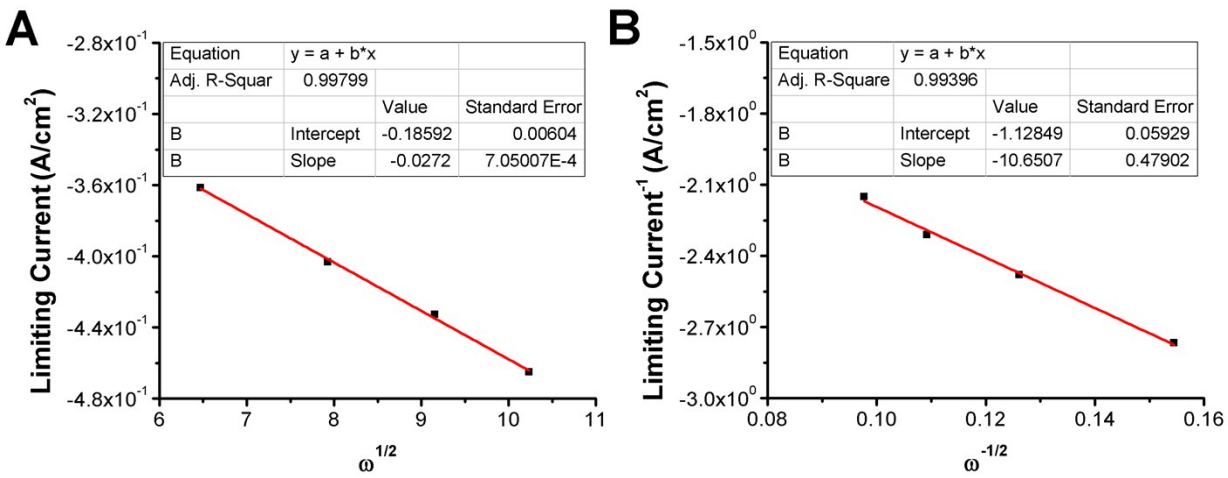

Figure S57. Levich **(A)** and Koutecky-Levich **(B)** plots from data obtained from Linear Sweep Voltammograms of $[Mn(TMPyP)Cl]^{4+}$ (0.25 mM) by RRDE under O_2 saturation conditions at various rotation rates in a pH 5 buffer solution.

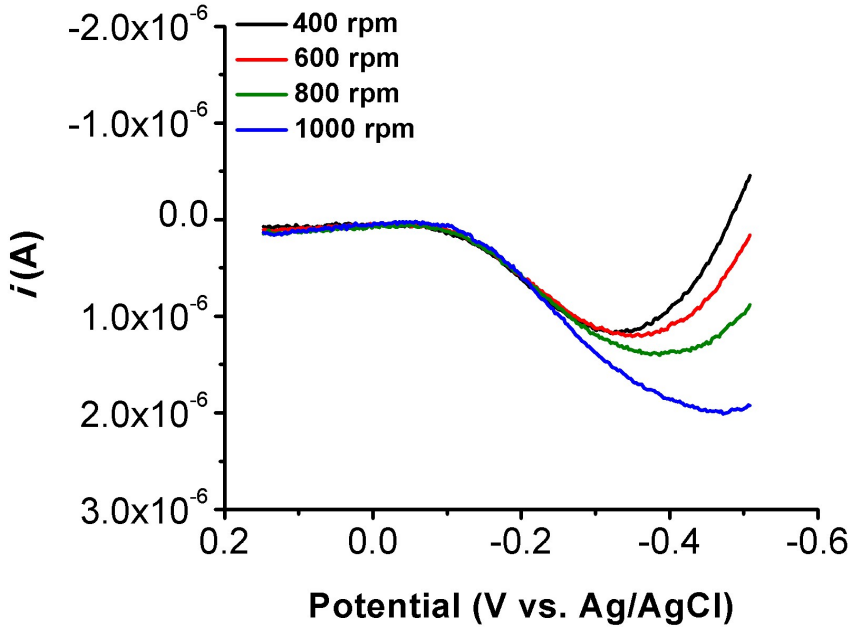

Figure S58. Linear Sweep Voltammograms of the generated ring current during RRDE experiments with $[Mn(TMPyP)Cl]^{4+}$ (0.25 mM) at various rotation rates with the argon ring current subtracted from the ring current produced under O_2 saturation conditions in a pH 5 buffer solution; ring potential = 1.2 V vs Ag/AgCl. Conditions: 0.25 mM analyte; glassy carbon working electrode/Pt ring working electrode, glassy carbon counter electrode, Ag/AgCl/3 M KCl reference electrode; scan rate 0.02 V/s.

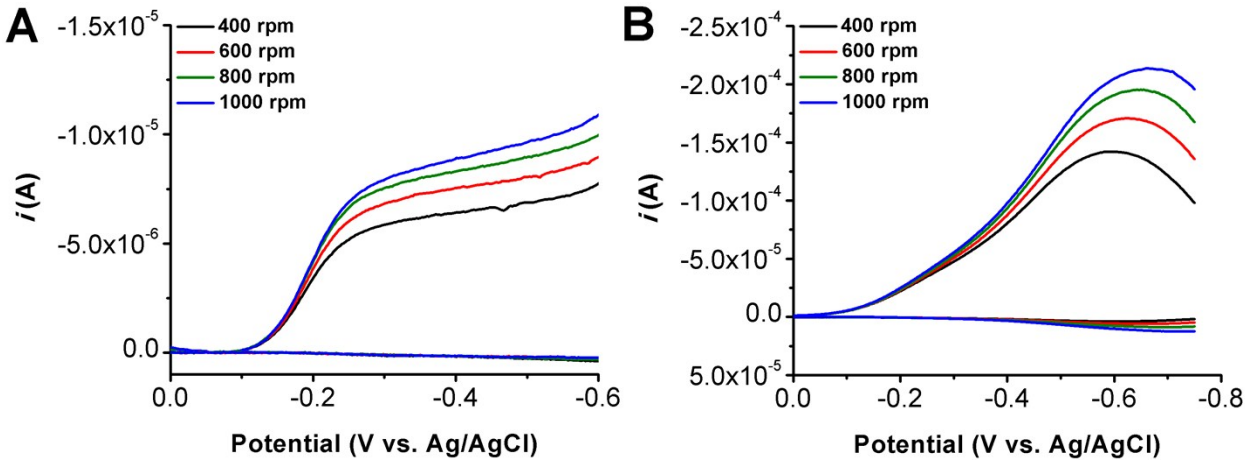

Figure S59. Linear Sweep Voltammograms of RRDE experiments with $[Mn(TMPyP)Cl]^{4+}$ (0.25 mM) at various rotation rates under argon **(A)** and O_2 **(B)** saturation conditions in a pH 6 buffer solution; ring potential = 1.2 V vs Ag/AgCl. Conditions: 0.25 mM analyte; glassy carbon working electrode/Pt ring working electrode, glassy carbon counter electrode, Ag/AgCl/3 M KCl reference electrode; scan rate 0.02 V/s.

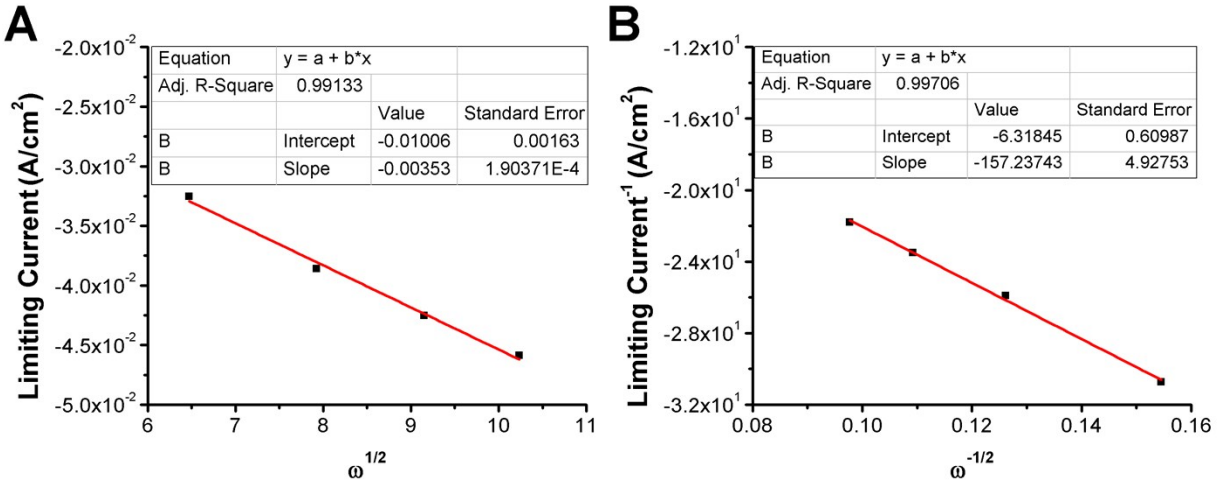

Figure S60. Levich **(A)** and Koutecky-Levich **(B)** plots from data obtained from Linear Sweep Voltammograms of $[Mn(TMPyP)Cl]^{4+}$ (0.25 mM) by RRDE under argon saturation conditions at various rotation rates in a pH 6 buffer solution.

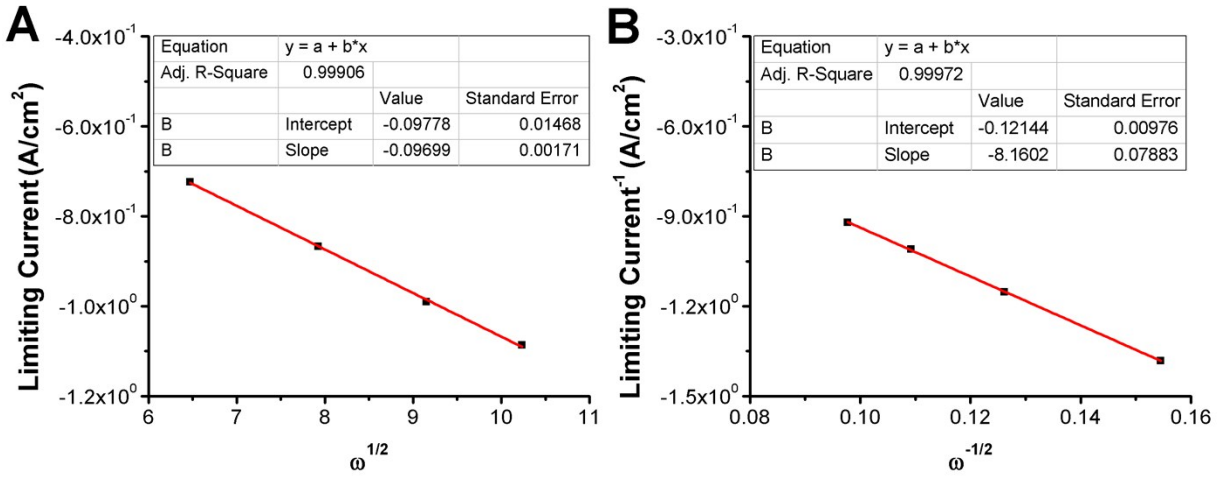

Figure S61. Levich **(A)** and Koutecky-Levich **(B)** plots from data obtained from Linear Sweep Voltammograms of $[Mn(TMPyP)Cl]^{4+}$ (0.25 mM) by RRDE under O_2 saturation conditions at various rotation rates in a pH 6 buffer solution.

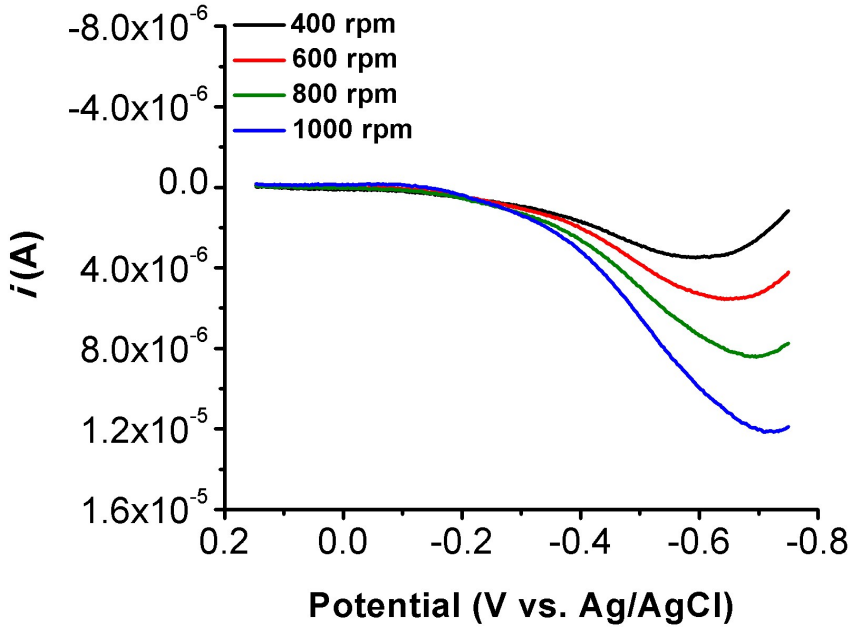

Figure S62. Linear Sweep Voltammograms of the generated ring current during RRDE experiments with $[Mn(TMPyP)Cl]^{4+}$ (0.25 mM) at various rotation rates with the argon ring current subtracted from the ring current produced under O_2 saturation conditions in a pH 6 buffer solution; ring potential = 1.2 V vs Ag/AgCl. Conditions: 0.25 mM analyte; glassy carbon working electrode/Pt ring working electrode, glassy carbon counter electrode, Ag/AgCl/3 M KCl reference electrode; scan rate 0.02 V/s.

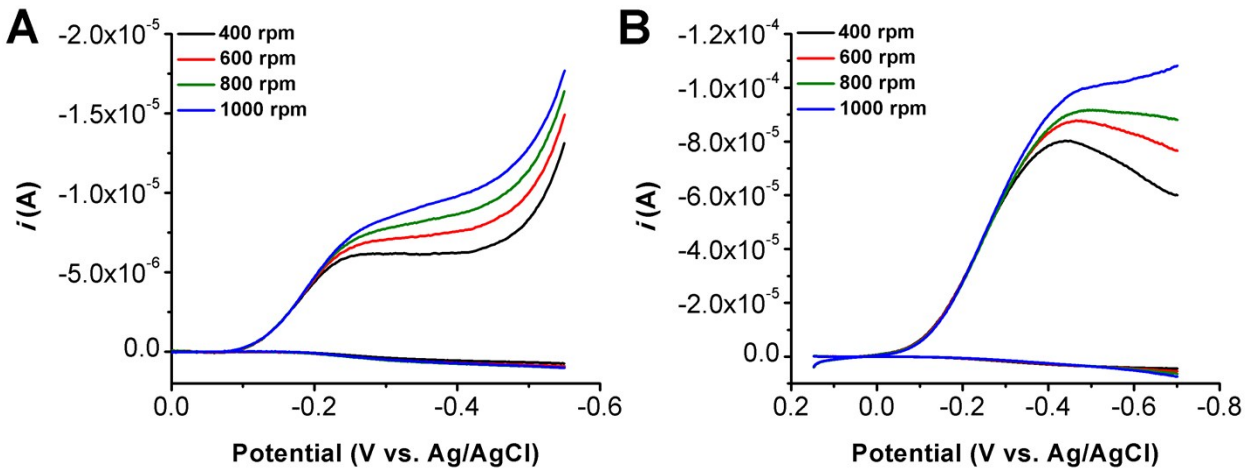

Figure S63. Linear Sweep Voltammograms of RRDE experiments with $[Mn(TMPyP)Cl]^{4+}$ (0.25 mM) at various rotation rates under argon **(A)** and O_2 **(B)** saturation conditions in a pH 4 buffer solution; ring potential = 1.2 V vs Ag/AgCl. Conditions: 0.25 mM analyte; glassy carbon working electrode/Pt ring working electrode, glassy carbon counter electrode, Ag/AgCl/3 M KCl reference electrode; scan rate 0.02 V/s.

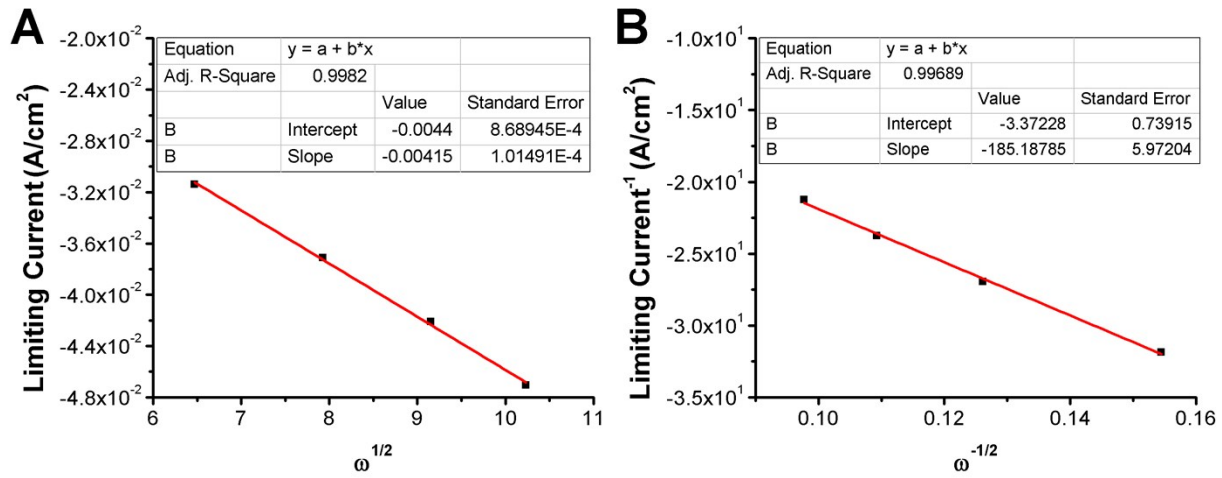

Figure S64. Levich **(A)** and Koutecky-Levich **(B)** plots from data obtained from Linear Sweep Voltammograms of $[Mn(TMPyP)Cl]^{4+}$ (0.25 mM) by RRDE under argon saturation conditions at various rotation rates in a pH 4 buffer solution.

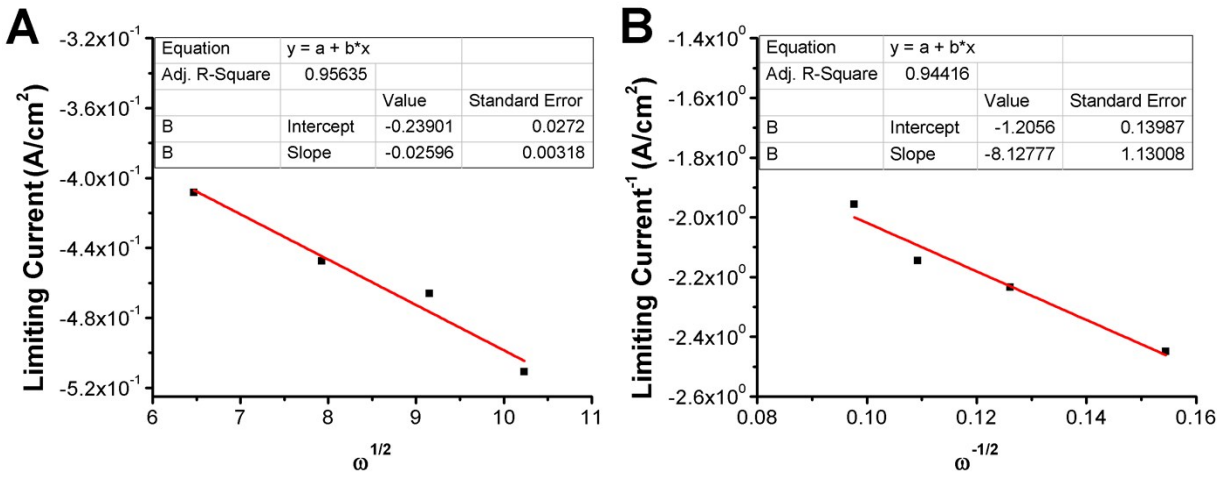

Figure S65. Levich **(A)** and Koutecky-Levich **(B)** plots from data obtained from Linear Sweep Voltammograms of $[Mn(TMPyP)Cl]^{4+}$ (0.25 mM) by RRDE under O_2 saturation conditions at various rotation rates in a pH 4 buffer solution.

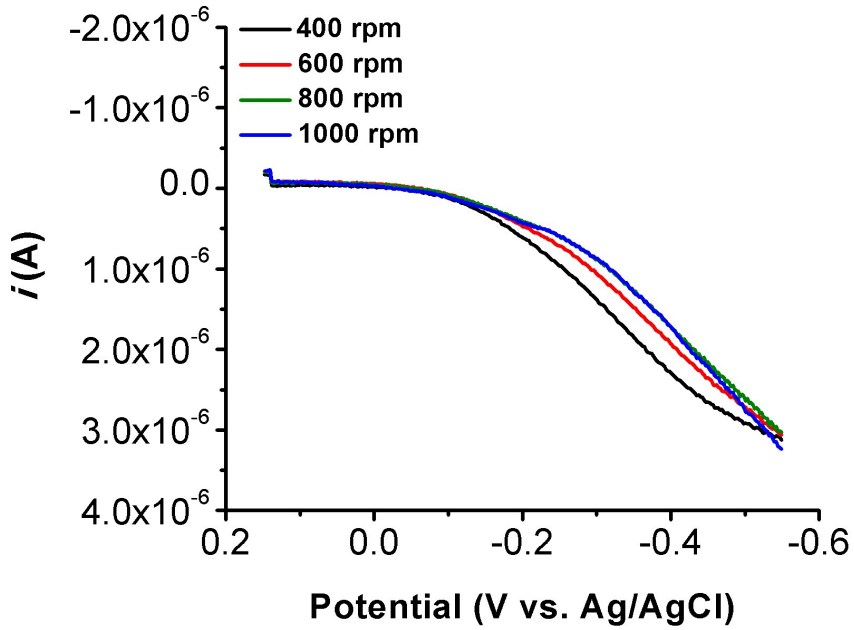

Figure S66. Linear Sweep Voltammograms of the generated ring current during RRDE experiments with $[Mn(TMPyP)Cl]^{4+}$ (0.25 mM) at various rotation rates with the argon ring current subtracted from the ring current produced under O_2 saturation conditions in a pH 4 buffer solution; ring potential = 1.2 V vs Ag/AgCl. Conditions: 0.25 mM analyte; glassy carbon working electrode/Pt ring working electrode, glassy carbon counter electrode, Ag/AgCl/3 M KCl reference electrode; scan rate 0.02 V/s.

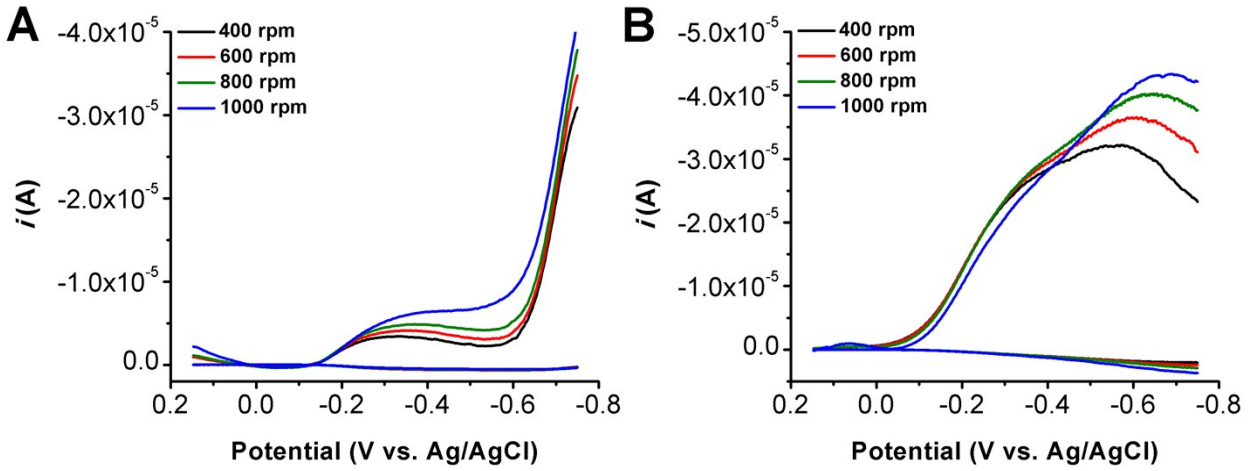

Figure S67. Linear Sweep Voltammograms of RRDE experiments with $[Mn(TMPyP)Cl]^{4+}$ (0.25 mM) at various rotation rates under argon **(A)** and O_2 **(B)** saturation conditions in a pH 3 buffer solution; ring potential = 1.2 V vs Ag/AgCl. Conditions: 0.25 mM analyte; glassy carbon working electrode/Pt ring working electrode, glassy carbon counter electrode, Ag/AgCl/3 M KCl reference electrode; scan rate 0.02 V/s.

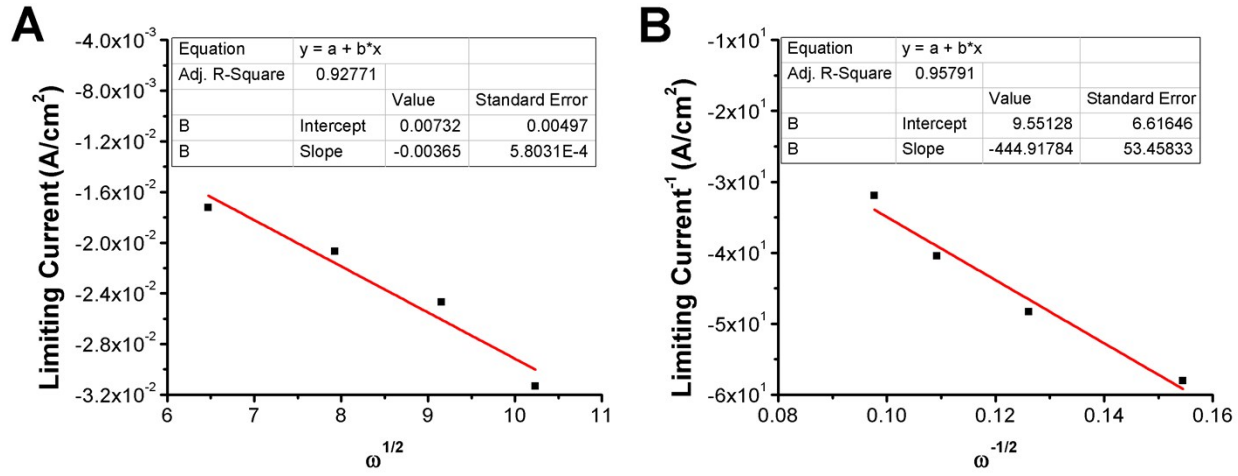

Figure S68. Levich **(A)** and Koutecky-Levich **(B)** plots from data obtained from Linear Sweep Voltammograms of $[Mn(TMPyP)Cl]^{4+}$ (0.25 mM) by RRDE under argon saturation conditions at various rotation rates in a pH 3 buffer solution.

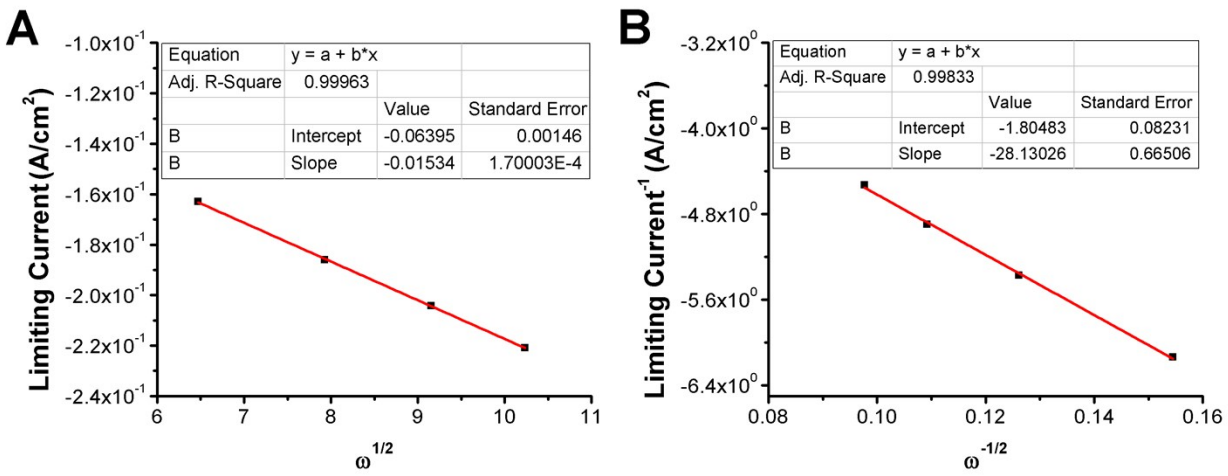

Figure S69. Levich **(A)** and Koutecky-Levich **(B)** plots from data obtained from Linear Sweep Voltammograms of $[Mn(TMPyP)Cl]^{4+}$ (0.25 mM) by RRDE under O_2 saturation conditions at various rotation rates in a pH 3 buffer solution.

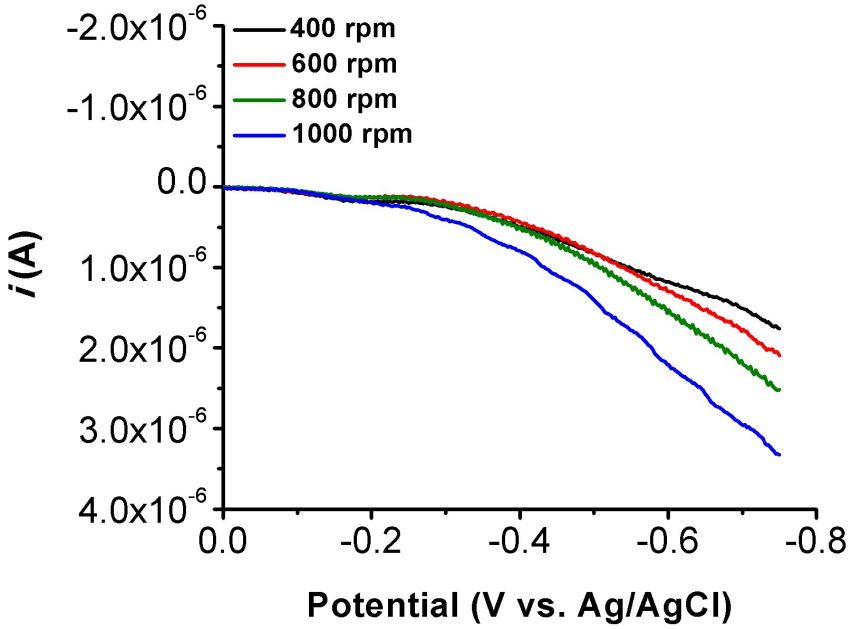

Figure S70. Linear Sweep Voltammograms of the generated ring current during RRDE experiments with $[Mn(TMPyP)Cl]^{4+}$ (0.25 mM) at various rotation rates with the argon ring current subtracted from the ring current produced under O_2 saturation conditions in a pH 3 buffer solution; ring potential = 1.2 V vs Ag/AgCl. Conditions: 0.25 mM analyte; glassy carbon working electrode/Pt ring working electrode, glassy carbon counter electrode, Ag/AgCl/3 M KCl reference electrode; scan rate 0.02 V/s.

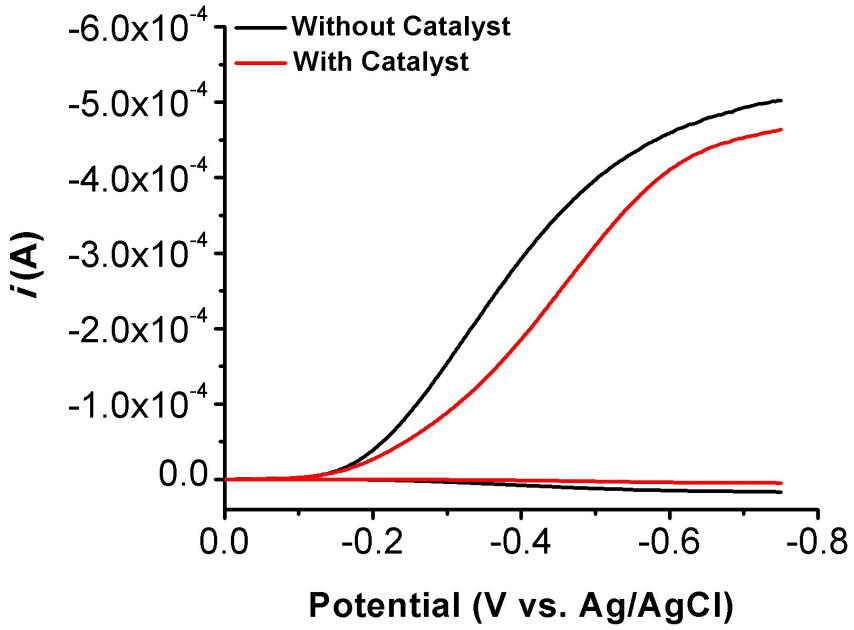

Figure S71. Linear Sweep Voltammograms of RRDE experiments with $[Mn(TMPyP)Cl]^{4+}$ (0.25 mM) at 1000 rpm under O_2 saturation conditions in a pH 7 buffer solution illustrating the inability to perform RRDE analysis above pH 6 due to the greater background disk and ring current observed at pH 7; ring potential = 1.2 V vs Ag/AgCl. Conditions: 0.25 mM analyte; glassy carbon working electrode/Pt ring working electrode, glassy carbon counter electrode, Ag/AgCl/3 M KCl reference electrode; scan rate 0.02 V/s.

Table S16. $\%H_2O_2$ calculated from RRDE experiments at various pH values.

pH	Rotation Rate (rpm)	$\%H_2O_2$	Average $\%H_2O_2$
3	400	16.2	
	600	15.4	
	800	17.4	
	1000	23.7	18 (±4)
4	400	14.0	
	600	11.4	
	800	10.4	
	1000	9.45	11 (±2)
5	400	6.71	
	600	6.14	
	800	6.77	
	1000	8.96	7 (±1)
6	400	9.64	
	600	12.8	
	800	16.9	
	1000	22.3	15 (±5)

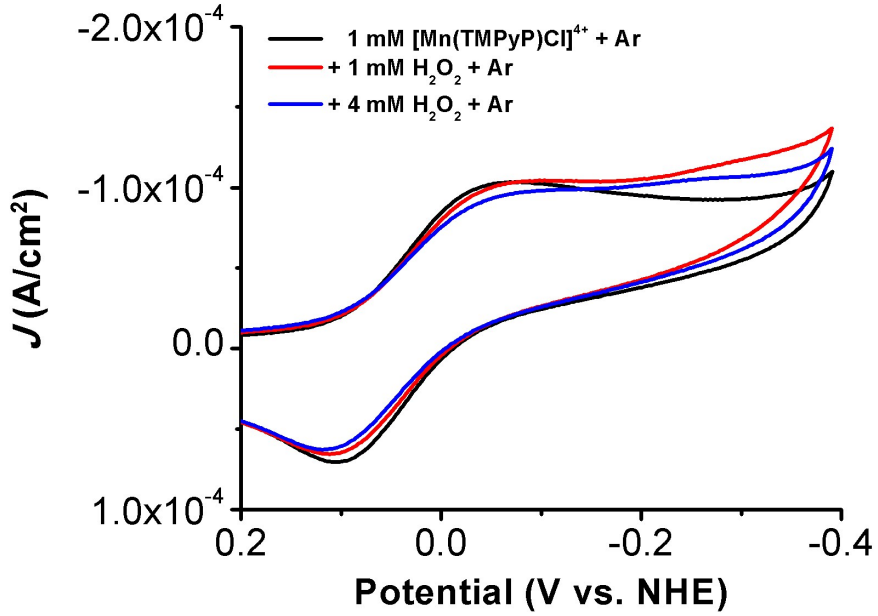

Figure S72. Control CV of 1 mM $[Mn(TMPyP)Cl]^{4+}$ with 1 mM H_2O_2 (red trace) and 4 mM H_2O_2 (blue trace) to show catalytic response for the dismutase of H_2O_2 in a pH 3 Britton-Robinson Buffer. Conditions: Glassy carbon working electrode, glassy carbon counter electrode, 3.0 M NaCl Ag/AgCl reference electrode; scan rate 100 mV/s.

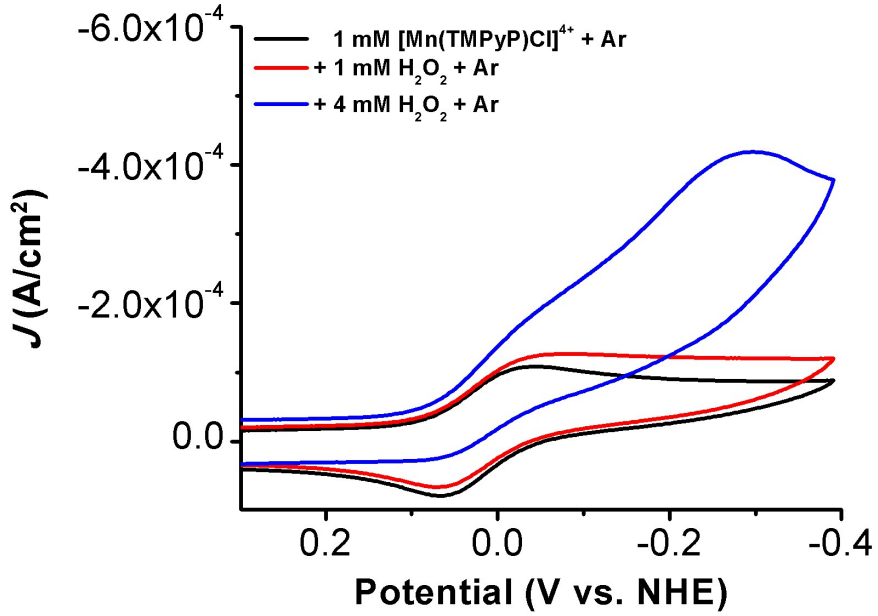

Figure S73. Control CV of 1 mM $[Mn(TMPyP)Cl]^{4+}$ with 1 mM H_2O_2 (red trace) and 4 mM H_2O_2 (blue trace) to show catalytic response for the dismutase of H_2O_2 in a pH 6 Britton-Robinson

Buffer. Conditions: Glassy carbon working electrode, glassy carbon counter electrode, 3.0 M NaCl Ag/AgCl reference electrode; scan rate 100 mV/s.

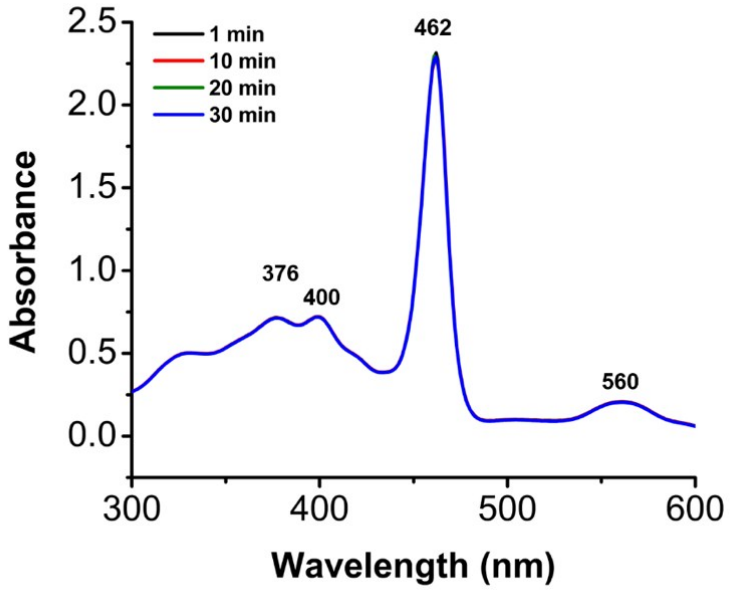

Figure S74. Control UV-Vis of 1.5 x 10^{-5} M $[Mn(TMPyP)Cl]^{4+}$ and 5.0 x 10^{-5} M H_2O_2 in pH 3 Britton-Robinson buffer.

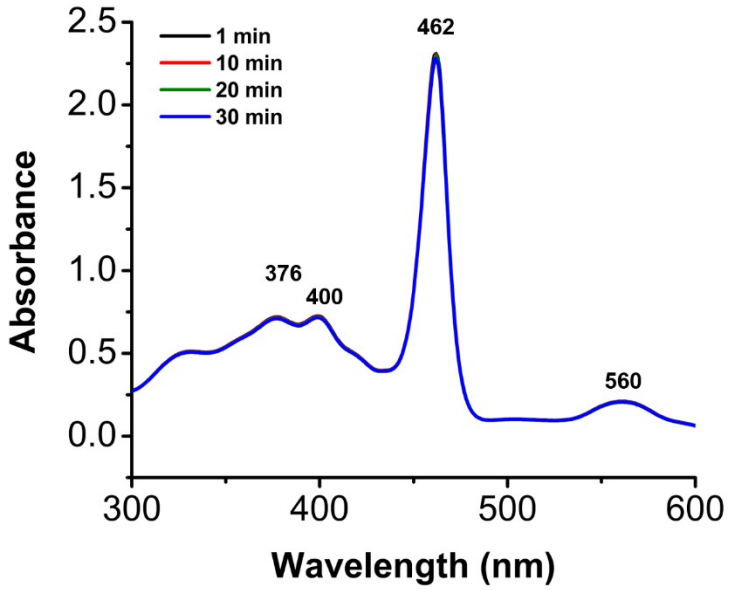

Figure S75. Control UV-Vis of 1.5 x 10^{-5} M $[Mn(TMPyP)Cl]^{4+}$ and 5.0 x 10^{-5} M H_2O_2 in pH 6 Britton-Robinson buffer.

References

1. Britton, H. T. S.; Robinson, R. A., CXCVIII.—Universal buffer solutions and the dissociation constant of veronal. *J. Chem. Soc.* **1931,** (0), 1456-1462.